MICROSTRUCTURAL CHARACTERIZATION OF SINTERED W-Ni-Cu ALLOYS

By

Kausik Chattopadhyay

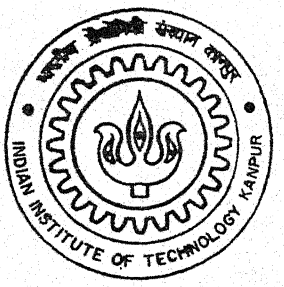

DEPARTMENT OF MATERIALS AND METALLURGICAL ENGINEERING

Indian Institute of Technology Kanpur

APRIL, 2003

MICROSTRUCTURAL CHARACTERIZATION OF SINTERED W-Ni-Cu ALLOYS

A Thesis Submitted

In Partial Fulfillment of the Requirements

For the degree of

Master of Technology

by

Kausik Chattopadhyay
(Roll No. Y110609)

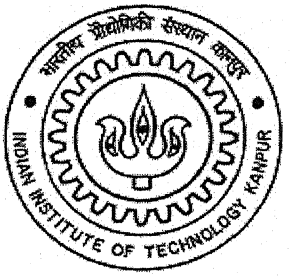

to the

DEPARTMENT OF MATERIALS AND METALLURGICAL ENGINEERING

INDIAN INSTITUTE OF TECHNOLOGY, KANPUR

APRIL 2003

CERTIFICATE

It is certified that the work contained in the thesis entitled "**Microstructural Characterization of Sintered W-Ni-Cu Alloys**" by **Kausik Chattopadhyay (Roll No. Y110609)**, has been carried out under our supervision and to the best of our knowledge this work has not been submitted elsewhere for a degree.

Dr. A. Upadhyaya
Assistant Professor
Department of Materials and
Metallurgical Engineering
Indian Institute of Technology
Kanpur

Dr. S. Sangal
Professor
Department of Materials and
Metallurgical Engineering
Indian Institute of Technology
Kanpur

ABSTRACT

The properties of sintered tungsten heavy alloys strongly depend on several microstructural attributes such as tungsten volume fraction, grain size, W-W contact area, and dihedral angle distribution etc. This study focuses on the effect of chemistry and sintering temperature on the microstructural parameters and the distortion behavior during liquid phase sintering of W-Ni-Cu alloys. These alloys contain 80, 85 and 90-wt% of tungsten with varying amounts of nickel to copper ratio (6:4, 7:3, 8:2). Quantitative metallographic measurements were performed on samples liquid phase sintered at two different temperatures 1440°C and 1460°C. The parameters measured include contiguity, connectivity, volume fraction of solid, average grain size, surface area per unit volume, and mean dihedral angle. The liquid phase sintered microstructure was compared with those obtained by solid-state sintering at 1360°C. An automated methodology has been developed to measure the dihedral angle of tungsten based heavy alloys on two-dimensional microstructure. This unique method provides a large and an accurate statistical estimate of the distribution of dihedral angles. The change of Ni:Cu ratio affects the dihedral angle and thereof microstructure, structural rigidity, and mechanical properties. The results of this investigation suggest that a low intersolubility and a high mean dihedral angle result in a more contiguous skeletal structure.

Table of Contents

List of Figures

List of Tables

Acknowledgements

I would like to express my deep gratitude to Dr. A. Upadhyaya and Dr. S. Sangal for their expert guidance, support and encouragement through out my graduate studies at Kanpur. Their leadership was immeasurable help to my early identification of an industrially significant area of research.

I gratefully acknowledge the help received from Mr. S. C. Soni and Dr. Mungole for providing me with guidance and letting me benefit from their experience during the experimental work.

My time at the P/M lab was enriched by the interaction with my fellow students. I am thankful to Sanjib, Maya, Sukanta, Sankar, Puspender, Chiradeep, Amit, Anirban, Pampa, and Puneet. Many of them are my close friends and I hope to keep for life.

I must acknowledge the support provided by my beloved parents, brothers and sisters. I would not have come this far without their unconditional love and support. This thesis is dedicated to them.

Last but not the least, I extend my special thanks to all the staff of Materials and Metallurgical Department and Advanced Center for Materials Science, for their unconditional help.

Kausik Chattopadhyay
IIT, Kanpur
April, 2003

Chapter 1

INTRODUCTION

Tungsten metal exhibits outstanding thermal properties, which makes it attractive for a broad range of applications. However, for certain applications its electrical and thermal conductivity, sensitivity toward oxidation and poor weldability are unsatisfactory. These limitations have led to the development of two-phase alloys. In these alloys the useful properties of tungsten are combined with those of the additives.

The term tungsten heavy alloys are used for a group of two-phase composites, based on Ni-Cu, Ni-Fe, and Fe-Co matrix. High density (16 to 18.6 g/cm3) and a unique combination of strength (700-1000 MPa) and ductility (5-20%) characterize them. Generally, these heavy alloys contain 80-98% tungsten and the balance being transition metals such as iron, cobalt, nickel and copper.

In addition of superior mechanical properties, these alloys also have good machinibility, and appreciable corrosion resistance. Because of refractoriness of tungsten liquid phase sintering is the only mechanism to produce these alloys. Sintered microstructure of heavy alloys comprises of rounded tungsten grains (20 to 60 μm), which are embedded in the matrix. Figure 1 shows a sintered microstructure of 90W-7Ni-3Fe alloy. While the grains are nearly pure bcc tungsten, the fcc binder matrix contains about 20% dissolved tungsten in solid solution. To achieve the desired properties of these heavy alloys several microstructural attributes such as solid volume fraction grain size, W-W contact area, contiguity and connectivity have to be optimized. In addition to these microstructural parameters, the properties of polycrystalline two-phase materials also depend on the grain boundary energy (solid-solid interfacial energy). The grain boundary energy states influence the strengthening properties of polycrystal significantly. Liquid phase microstructures are invariably two-phase microstructure. Hence, in addition to the solid-solid interfacial energy (grain boundary energy) the solid-liquid interfacial energy too has to be accounted for. The balance of these two energies defines the extent of melt penetration along the grain boundary. This can be quantified by dihedral angle. The dihedral angle is directly related to the other microstructural parameters such as contiguity, connectivity, which in turn determines the physical and mechanical properties

of these alloy systems. Two-dimensional measurement of dihedral angle is the best estimate of the true value. This is very tedious and time-consuming process. In order to have an accurate and fast measurement of dihedral angle, an automated technique has been developed. This is a unique process. The efficacy of this technique has been tested on W-Ni-Cu and W-Ni-Fe alloys. The application of digital data processing has enabled us to process statistically adequate number of data in reasonable time, and accuracy level is increased. In this work, we have investigated the effect of tungsten, binder content, and temperature on W-Ni-Cu alloys. We have quantified the microstructures of W-Ni-Cu alloys.

Chapter 2 gives the background of our studies. This includes the phase diagram of Cu-Ni isomorphous system, introduction of tungsten heavy alloys, powder metallurgy processing of W-Ni-Cu alloys and effects of different parameters on properties of heavy alloys. Finally, different aspects of microstructural characterization are discussed.

Chapter 3 scope of our present work is discussed. This includes the reason for system selection, the effect of sintering temperature and binder phase composition on microstructure evolution.

Chapter 4 describes in detail the experimental procedures. In includes sample preparation, density measurement, and quantative measurement. It also describes the image processing for automated dihedral angle measurement.

Chapter 5 describes the experimental results. Chapter 6 and 7 consist of discussion and conclusions respectively.

Chapter 2

BACKGROUND

2.1 Tungsten Heavy Alloys

Tungsten is a metallic transition element. It is a vital industrial material with a rich history that spans over several centuries. An outstanding characteristic of tungsten is its high melting point of over 3400°C, which exceeds that of all other metals. The high melting point of tungsten indicates the exceptionally strong cohesion between the atoms of the metal. This also accounts for the great strength at ambient and elevated temperature. It has also very small thermal expansion. Tungsten, not only has the highest melting point but also the lowest vapor pressure of all refractory materials. Low thermal expansion of this metal accounts for a number of applications. It has the advantage that its expansion coefficient remains low up to the melting point, increasing linearly with temperature [1]. The electrical resistance properties of this metal are important for heating elements for high temperature furnaces. It also exibihits outstanding thermal properties, which makes it attractive to be useful over a broad range of applications. However, for some applications its electrical and thermal conductivity, sensitivity towards oxidation, and poor workability are unsatisfactory. These limitations have led to the development of two-phase alloys, in which the useful properties are combined with those of the additives.

Tungsten heavy alloys with densities between 16.1 and 18.3 g/cm^3 represents the heaviest materials generally available to the engineers. Whilst more dense materials exist (U 19.05 g/cm^3, W 19.32 g/cm^3, Au 19.30 g/cm^3 and platinum group metals with densities ranging from 20.5 - 22.48 g/cm^3), their use is restricted by availability, workability and cost [2,3].

A typical tungsten heavy alloy contains 80-98 wt. % tungsten with a balance of relatively low melting transition elements, such as iron, cobalt, nickel, and copper. Tungsten heavy alloys exhibit tensile strength between 700-1000 MPa and have ductilites between 5-20% [3].

These alloys are mostly consolidated through powder metallurgy technique. Thus, it is possible, either to press components to shape, or to cut and shape materials prior to sintering. This ability to produce parts very close to the materials size reduces the amount of final machining necessary to produce the finished components. Tungsten heavy alloys can be machined without much difficulty.

Tungsten heavy alloys are processed through powder metallurgy route since 1930's [4]. These alloys contain mainly pure tungsten as principle phase in association with binder phase containing transition elements (Fe, Co, Ni, Cu) [2]. Figure 2.1 shows the optical micrograph of a tungsten heavy alloy. Depending upon the binder composition, heavy metals can be classified into two main groups [1]:

(a) W-Ni-Fe

This group is ferromagnetic. The nickel to iron ratio typically range between 1:1 to 4:1. The preferred ratio is 7:3, since this composition avoids the formation of intermetallic phases. W-Ni-Fe alloys exhibit excellent strength ductility combinations. It can be cold worked to a reduction of 60% without intermediate annealing.

(b) W-Ni-Cu

Members of this group are non-magnetic and exhibit a higher electrical conductivity. The nickel to copper ratio ranges from 3:2 to 4:1. These alloys exhibit lower strength and ductility than W-Ni-Fe alloys.

These heavy alloys have excellent resistance to most of the common corrosive agents; in dilute solutions of HCl, resistance to attack is up to twice that of 18/8 stainless steel. It remains stable up to temperature 1000°C and good oxidation resistance up to 400°C [3].

The unique properties of heavy alloys together with its machinibility make it one of the more versatile materials available to the engineers. Its uses can be broadly split into three categories yet new applications are still being explored.

The high density and strength of these materials make it an ideal choice in the use of balance weights in

- Aircraft mass balance weights
- Control surface balance weights
- Counter balance weights
- Flywheel weights
- Crank shaft, particularly high performance racing engines

The densities of these alloys make it a suitable candidate where energy absorption is required. It is used to mount sensitive running equipment to eliminate vibration. The same anti-vibration characteristics are employed in tool shank material for boring bars and grinding quills. The electronic industry also uses heavy alloys in transducer.

Because tungsten heavy alloys are much denser than that other shielding materials a reduction in the volume of a shield is possible allowing a saving in space and in many cases weights. It is used throughout medical and nuclear industries.

- Collimators
- Directional shields on radiation detection equipments
- Gamma and X-ray camera shutters
- Isotopes transport
- Radiotherapy equipments
- Syringe shields and containers

In short, we can summarize the properties that make the heavy alloys a versatile product are as follows:

- The high modulus of elasticity (much high than steel)
- Excellent vibration damping characteristics
- Good machinibility
- High absorption ability for X-rays and γ-rays
- Good thermal and electrical conductivity
- Low electrical erosion and welding tendency
- Good corrosion resistance

2.2 Recent Developments

Recent efforts have focused on improving the strength and hardness of heavy alloys at the expense of ductility, which requires strengthening through alloying additions and microstructural control. The attention was diverted to other binder such as Fe-Ni from Cu-Ni binder because of better mechanical properties. Generally, the tungsten based heavy alloys are W-Ni-Cu, W-Ni-Fe, W-Ni-Co, and W-Ni-Cr. Because of higher cost of cobalt, W-Ni-Co alloys are costly. However, cobalt as a ternary addition in the binder of W-Ni-Fe heavy alloys has been reported [5]. Straight nickel binder proved to be better as compared to the binary Co-Ni binders as far as the mechanical properties were concerned. W-Cr-Ni alloys exhibited superior hardness values as compared to the conventional W-Ni-Cu and W-Ni-Fe alloys. These alloys also exhibited high ultimate tensile strength along with the poor ductility values. Later on, refractory elements were added with tungsten to improve strength and hardness. The effective alloying addition includes Ta, Mo, and Re that have total solubility in

tungsten and high solubility in matrix [6]. As a result, it gives grain size refinement with improved strength and hardness. Addition of Cr, V, and Nb provide improved strengthening effect. But these elements have densities lower than the tungsten, thus even though the strength and hardness are increased the theoretical density is lower. On the other hand, Re is a high density-alloying element that proves to be very effective in tungsten heavy alloy system due to its small atomic size as compared to tungsten.

However, from fundamental aspects, W-Ni-Cu system is an ideal system to investigate. The present research concentrates on W-Ni-Cu alloys containing 80, 85, 90-wt% W with nickel to copper ratio 6:4, 7:3, 8:2.

2.3 Fabrication:

Heavy alloys are fabricated by conventional P/M technique. The flow chart for a typical fabrication process of tungsten heavy alloy is given below [1].

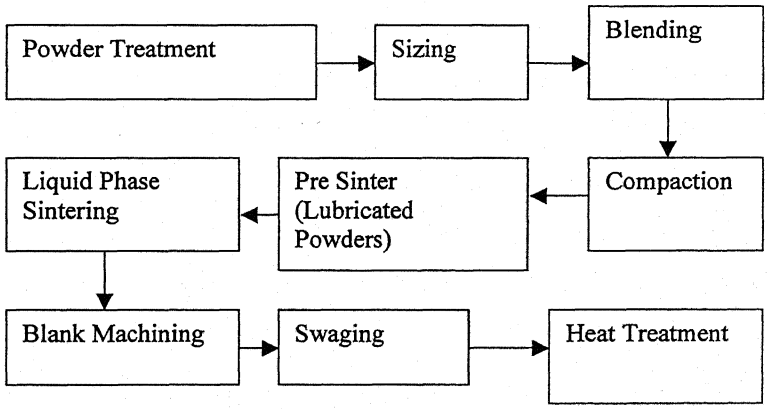

Tungsten heavy alloys are typically formulated from elemental powders with mean particles sizes in the range of 1.5 to 7 μm. Blend homogeneity is essential for microstructural uniformity and predictable sintering to full density. They are commonly processed to full density by solid-state sintering or liquid phase sintering in hydrogen atmosphere. Liquid phase provides a superior densification than solid-state sintering. The liquid phase microstructure consists of spheroids of nearly pure tungsten in the binder phase of transition metals plus dissolved tungsten. Post sintering process plays an important role in improving the mechanical properties of these alloys. Using pure powders and post sintering heat treatments that involves quenching from high temperatures controls impurity segregation and embrittlement of

interfaces. Changing gases within sintering cycle controls hydrogen embrittlement. The sintering atmosphere plays a vital role in controlling the residual porosity.

During sintering on cooling a significant amount of tungsten remains in solid solutions depending upon the binder composition and cooling rate. The solubility of tungsten is the highest in W-Ni alloys (typically 40 wt%), making the alloy low ductile in nature. But addition of copper, iron depress it to lower values (typically 20 to 25 wt% W). This results a tough and ductile binder matrix.

2.4 P/M processing of W-Ni-Cu alloys

Powder metallurgy (P/M) is the study of the processing of metal powders that involves fabrication, characterization and conversion of metal powders into useful engineering components. P/M method is one of the most modern methods known for fabrication of metal components. For the last few decades, powder metallurgy method is the most promising and emerging field to produce materials with novel properties that cannot be produced by any other technique [7]. The evolution of powder metallurgy industry originated as a means fabricating refractory metals (W, Nb, Mo, Zr, Ti, and Re). This is quite difficult to fabricate these high melting points metals by other techniques. In fact, tungsten has an historical link with powder metallurgy for many decades [8].

The P/M processing strategies includes application of pressure, deformation and heat to the powders. As a result of which the powders get shaped to a desired component with improved properties. This manufacturing process can be considered to be consist of three basic steps [9]:

a) Powder mixing
b) Powder compaction
c) Consolidation or sintering

Metal powders can be produced by physical, chemical, and mechanical methods. Typically tungsten powder is produced by reduction of its oxide. The temperature and time of reduction control the final powder size and its distribution. Copper and nickel powders can be produced by various techniques such as atomization and electrolysis etc. The addition of copper and nickel with tungsten reduces the sintering temperature. Powders are blended to meet the required specifications and mixed with a lubricant usually a metal stearate that aids

compaction. The compression of the powder in the closed die reduces the voids between the particles.

The pressed compact is given a thermal treatment named sintering under a protective atmosphere or in vacuum. Typically the sintering temperature range of W-Ni-Cu alloys is 1400 to 1500°C. The lubricant is evaporated and porosity is reduced by metal transport involving surface and volume diffusion. This leads to the chemical bonding between the particles. As sintering proceeds, the original interconnect porosity is reduced, closed pores are formed and the overall shrinkage is controlled to ensure the final densification of the compact.

2.5 Sintering:

Sintering is defined as a thermal treatment for bonding particles into a coherent predominantly solid structure via mass transport events that usually occurs at atomic level [10]. The driving force for sintering is the lowering of total surface energy, which occurs by reduction in surface area with concomitant formation of interparticle bonds. It can occur at temperatures below the melting point of major constituents. Generally, the bonding occurs due to the growth of cohesive necks at the particle contacts. Currently, several processing methods are being used for processing of tungsten heavy alloys, such as solid-state sintering, liquid phase sintering, arc casting, electron beam melting swaging, hot extrusion, hot explosive consolidation, chemical vapor deposition, powder injection molding and mechanical alloying. Here, we are confined mainly on solid-state and liquid phase sintering of W-Ni-Cu alloys.

2.5.1 Solid-State Sintering:

Sintering phenomena in the solid-state takes place during heating a powder up to the temperature for liquid phase sintering. The driving force for solid-state sintering is excess surface free energy. Sintering is a complex process and for any given metal and set of sintering conditions there are likely to be different stages and material transport mechanisms associated with this process. In the systems with solubility with the binder phase, such as W-Ni-Cu or W-Ni-Fe significant densification occurs in the solid-state. Figure 2.2 shows the ternary phase diagram of tungsten, copper, and nickel. It indicates that the phase ultimately produced in equilibrium with tungsten in the 5:2 alloy to be the solid α phase. The copper-nickel equilibrium diagram is

reproduced in figure 2.3, and it is too well know to need comment. But, in systems without solubility, such as W-Cu, the densification is small in both solid and liquid state. Earlier, researchers looked at full densified W-Ni-Cu composites by solid state sintering. Solid state activated sintering of tungsten powder with various Cu-Ni addition was studied by Brophy *et al.* [11]. Their study was mainly confined to densification mechanism. It was proposed that shrinkage occurs during the initial two stages of sintering: (i) rearrangement and (ii) solution-reprecipitation stages. The selected composition was 90W-5Cu-5Ni. The sintering was carried out from temperatures 1300-1350°C for different periods for each sintering temperature. The role of phase relationships on the activated sintering of tungsten was studied by Prill *et al.* [12]. They proposed that alloying nickel with copper diminishes the acceleration of sintering of tungsten. The studied composition was 99 wt% W-1wt% (Cu-Ni) with various ratios of copper to nickel in the binder. The main binder composition of interest was 75% Cu-25% Ni. They concluded that sintering follows two different mechanisms, one solution controlled and the other diffusion controlled. Another part of the investigation made by them was to vary the overall Cu-Ni binder from 0.1%-3.0% keeping the Cu:Ni ratio as 3:1 in all the cases. They concluded that the bulk increase in matrix had no effect on shrinkage, when an optimum shrinkage was achieved.

2.5.2 Liquid Phase Sintering:

Liquid phase sintering is the most viable mechanism to produce these heavy alloys, where one can obtain almost theoretical density values. Liquid phase sintering is characterized by the presence of one or more than one liquid phase throughout or in part of sintering cycle. The formation of liquid phase during sintering usually increases the sintering rate. Liquid phase sintering has been practiced since 4000B.C, in various forms, largely in fabrication of pottery and glass-bonded ceramics, such as porcelain [10]. The tungsten heavy alloys (W-Ni-Cu, or W-Ni-Fe) in the 1930s provided an important theoretical basis of the process. When the pressed copper-nickel-tungsten powder mixture is heated, some copper melts at 1083°C without diffusion of nickel in the solid state. This liquid dissolves nickel and becomes solid. At a higher temperature more nickel is dissolved in the liquid, which then takes up tungsten and again solidifies. In this sense, sintering is accompanied by the presence of liquid. The presence of liquid promotes the faster rate of densification. The mass

transfer rate through the liquid is much higher than the solid. The capillary stressed due to wetting liquid results in rapid compact densification without the need for an external pressure. The liquid also aids to the rapid rearrangement of particles by reducing the friction. The liquid phase present in the system facilitates packing and high compact density.

In this type of sintering, it is generally desired to get complete densification during sintering. This means that amount of shrinkage will depend upon the green density of the compacts, since shrinkage is determined by the difference between green density and theoretical density of the material [13]. For the liquid phase sintering mechanism to be operative, it is necessary that the particles of the solids be quite fine. In materials where the percentage of the liquid phase at the sintering temperature is high, complete densification may be achieved in the first stage of the liquid phase sintering process. The liquid phase surrounds all the particles of the solid phase. The pores are imbedded in the liquid phase and are readily eliminated by a viscous flow process. A process in which the solid phase dissolves in the liquid, is transported through it by diffusion and is redeposited on the solid is necessary to get complete densification. In this case, the solid phase must be soluble in the liquid phase. This is the reason why the W-Cu-Ni heavy metal in which the solid phase, i.e., the tungsten, is soluble in the liquid phase, i.e., a copper-nickel alloy, densifies readily. Alloys of tungsten with copper alone, in which the solubility of solid tungsten in liquid copper is minimal, are difficult to densify by liquid phase sintering. The linear shrinkage during liquid phase sintering may as much as 10 to 15% that makes dimensional control more difficult in this type of sintering.

During microstructural evolution in liquid phase sintering, three stages are observed. They are- (1) particle rearrangement, during this period the liquid forms and wets the solid particles, (2) solid dissolution and reprecipitation resulting in grain shape accommodation and pore elimination, and (3) microstructure coarsening, causing an increase in the mean grain size with time to achieve a minimum surface energy per volume ratio [14,15]. The driving force for these three processes is the reduction in surface energy. The surface energy acts on the microstructure to achieve a minimum energy configuration. Good wetting is also a major concern in liquid phase sintering. Final densification is enhanced by a low solid-liquid surface energy, compared to the solid-vapor and liquid-vapor surface energies. Capillarity is also associated with interfacial energies. When the liquid forms, it can penetrate along the

tungsten particle contacts and grain boundaries such that strong attractive forces are exerted on the solid to cause rearrangement, densification and particle contact flattening [16]. An additional effect to consider is solubility; tungsten should be soluble in the liquid phase to enhance diffusion during sintering. Flow of tungsten in the liquid results in homogenization, pore elimination, and strengthening. A high solubility of the liquid in tungsten is unfavorable as it leads to pore formation and swelling. In the case of W-Ni-Cu system the liquid persists through out the sintering cycle as opposed to the transient liquid phase sintering.

Rearrangement

It involves large-scale bulk movement of particles within the liquid phase, which causes rearrangement and densification. Liquid flows through the pores and displaces the solid particles into the center of compact. During this stage capillary forces due to wetting liquid act on the particles and pool the particles into close proximity. The particles repacked closely as successive cluster of particles form and pores are eliminated by viscous flow. The presence of the liquid phase aid in smoothing the particle surface, thereby lubricating particle rearrangement [6]. The liquid further enhances the packing by attacking and disintegrating cluster of particles and repacking follows through redistribution of the small fragments between the big particles [16-18]. Increasing the amount of liquid phase leading to greater densification enhances particle movement. The driving force may be expressed in terms of surface energies/tensions, the greater the decrease in surface energy the better is the driving force for densification. Most heavy alloys densify to full density before the onset of liquid formation. Rearrangement process is hindered by high compaction pressure due to more W-W contacts that lock the particle into place [19]. Pore formation is due to inhomogeneous rearrangement and liquid flow from large to small capillaries resulting in a lower pore density with a higher mean porosity [20]. Researchers showed that rearrangement is a discontinuous process in W-Ni-Cu alloy [21,22]. After formation of rigid tungsten skeleton, only a fraction of single or small groups of particles are free to rearrange. In heavy alloy systems, W is soluble in Ni-Cu or Ni-Fe matrix and in the case of low heating rate considerable solid-state sintering takes place prior to rearrangement stage.

Solution Reprecipitation

Solution reprecipitation stage is also active during the rearrangement stage. However, it does not become dominant until the end of the first stage. Kingery showed that the driving force for this process is the difference in chemical potential arising from the pressure difference between the thin melt and the surrounding melt [15]. For solution reprecipitation to occur, the solid should have the solubility in the melt, such as in the W-Ni-Cu system. Therefore, the rate of densification in this stage is dependent on mass flow through the liquid. This stage also leads to densification, but at slower rate. The solubility of particles in the liquid phase increases by increasing the convexity (smaller size particles). Material transport by melt and subsequently reprecipitation on the coarser tungsten grains occurs called reprecipitation or Ostwald ripening mechanisms. Particle coalescence in this stage has been observed in the tungsten heavy alloy systems followed by neck formation. The growth of necks proceeds by mass transfer from small particles in the surrounding matrix and with a lesser extent from the redistribution of mass over the curved grain surface.

Microstructural Coarsening

A solid skeleton forms in this stage. However, solution reprecipitation still proceeds in systems where tungsten is soluble in the liquid phase, such as W-Ni-Cu system. As a consequence, grain growth, grain shape accommodation, and final stage pore removal follow because a solid skeleton exists between the solid grains and remaining pore elimination is dependent on diffusional relaxation of the skeleton [23]. Grain coalescence contributes to grain growth during final stage of liquid phase sintering. Dihedral angle plays an important role to promote densification in this stage. In case of dihedral angle>0, interface (solid-solid) is still stable. The elimination of pore is not high, so densification rate is very slow. But in this stage, there is no overlap of second stage possible. Therefore, amount of densification may be due to secondary accommodation.

If wetting of particles by the liquid phase is incomplete then there may be some solid particles in contact rather than separation. This leads to skeleton type of structure after densification. On the other hand, if the amount of liquid phase is more than sufficient then it may lead to "Sweating" [24]. So, for proper densification the amount of liquid phase and separation of solid particles through the liquid phase

should be controlled properly. Finally, all these stages of liquid phase sintering leads to full density compact and microstructural modification. The elimination of pores in this stage is dependent on the processing atmosphere and the nature of the vapor entrapped within.

Figure 2.4 shows the classical stages of liquid phase sintering involving mixed powders that form liquid on heating.

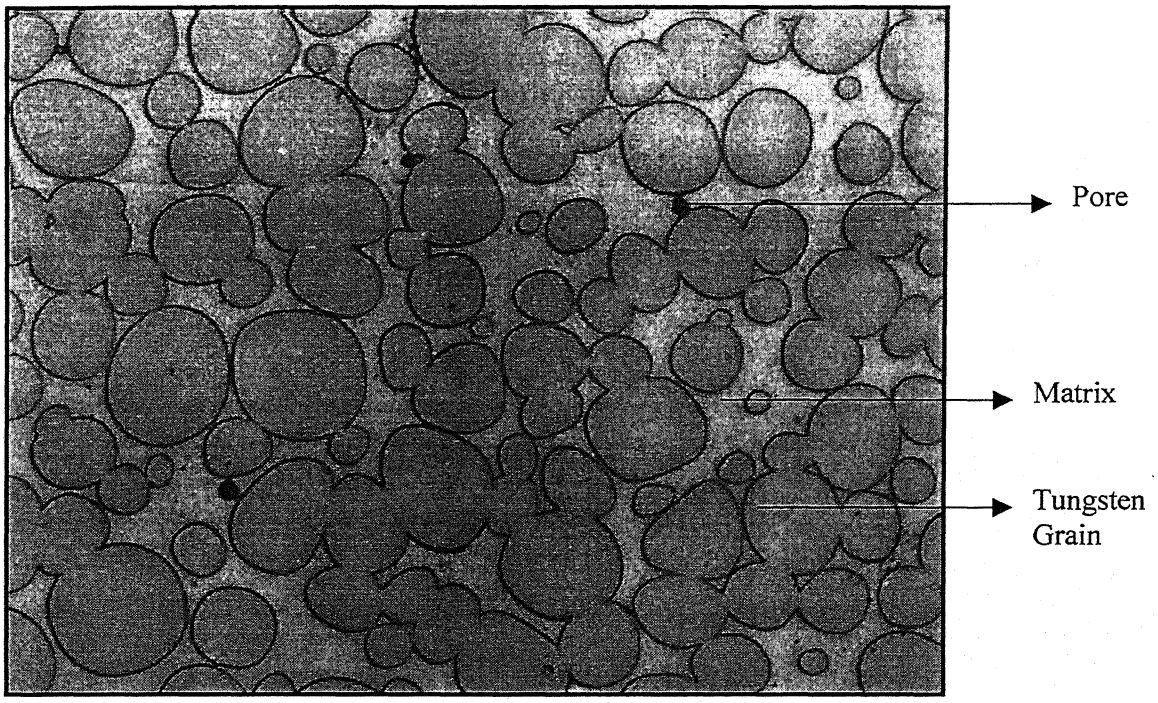

Figure 2.1. Optical Micrograph of a 90-wt% tungsten heavy alloy with 7-wt% Ni and 3-wt% Fe [24].

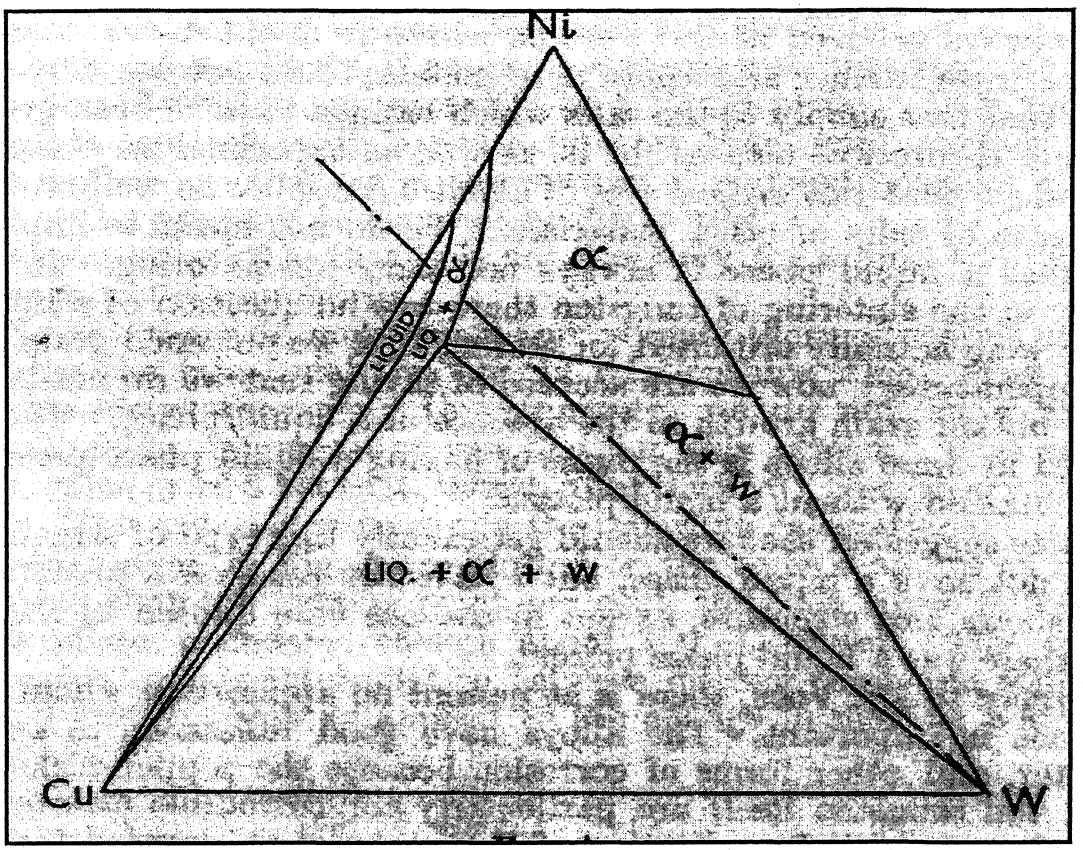

Figure 2.2 Ternary Phase Diagram of W-Ni-Cu alloys [28].

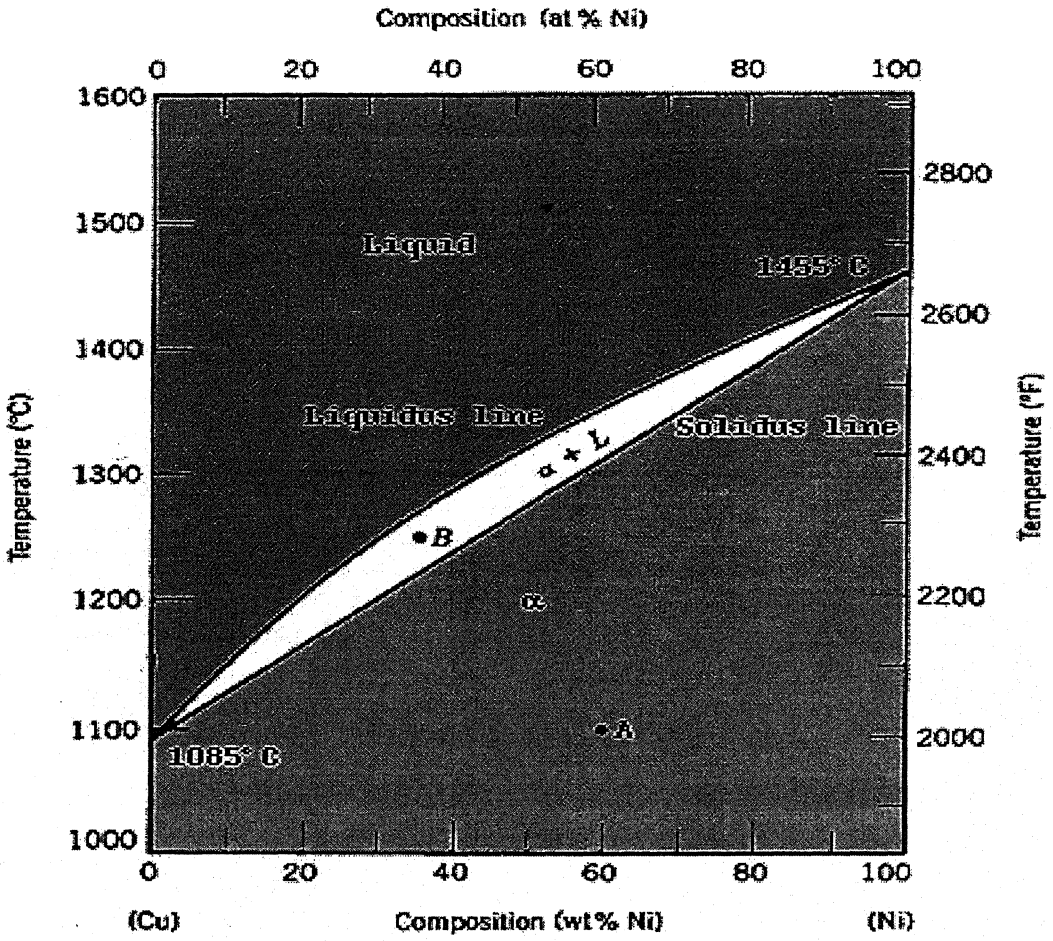

Figure 2.3 Copper-Nickel Equilibrium Phase Diagram [28].

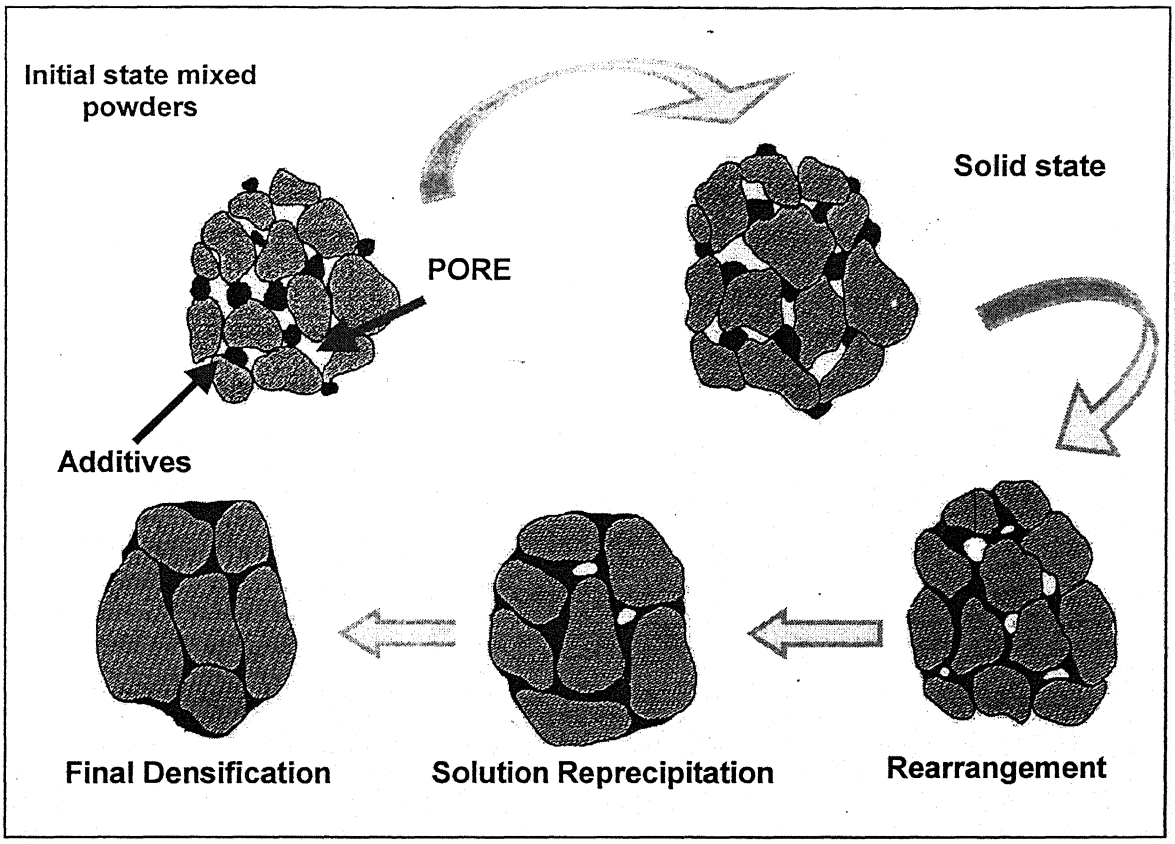

Figure 2.4. Classical Stages of Liquid Phase Sintering [6].

2.6 Effect of Sintering Condition on Microstructural Parameters of Tungsten Heavy Alloys

W-Ni-Cu alloys exhibit unique combination of high strength, density and ductility. Their mechanical properties especially ductility is more sensitive to sintering condition. Numerous research have been done on the effect of sintering temperature, sintering time and sintering atmosphere on the mechanical properties of tungsten heavy alloys. Processing conditions affect porosity, densification and grain growth, all of which eventually affects the final mechanical properties.

Volume fraction of matrix, grain size, dihedral angle and contiguity depend upon the sintering temperature. It has been reported that as sintering temperature increases the grain size and volume fraction of matrix increases while the contiguity and dihedral angle decreases [25,26]. The high sintering temperature results in the high solubility of tungsten in matrix, which in turn leads to more matrix phase. On the other hand, high sintering temperature leads to high diffusivity of tungsten in the matrix phase, which leads to faster tungsten grain growth rate. Moreover, high sintering temperature is responsible for low dihedral angle. A low dihedral angle corresponds to a lower contiguity. Thus, microstructure of heavy alloys changes with sintering temperature. At higher sintering temperature, there are few but large tungsten grain, more matrix and consequently greater free matrix path. As a result, the dislocation slip paths in the matrix are long and therefore less work hardening is present, which leads to lower strength and hardness. On the other hand, the increase in ductility is attributed to the more matrix, long dislocation slip path, less work hardening and low contiguity. At higher sintering temperature, the formation of large tungsten grains leads to initiation of larger crack at the tungsten-tungsten interfaces, which ultimately lead to decrease in ductility. It has been also observed that strength and ductility of tungsten heavy alloys decrease over given sintering period [27]. Early researchers showed that with increasing sintering time the tungsten grain contacts flatten and tungsten contiguity decreases.

2.7 Effect of Sintering Temperature on W-Ni-Cu

Cu-Ni was the first proposed binder for the liquid phase sintering of tungsten based heavy alloys by Price, Smithelles and Williams [28]. They showed that the

optimum composition depends on the choice of sintering conditions and would be nearer the tungsten corner of the ternary diagram if the time or the temperature were increased. Furthermore, it was shown that highly dense W-Ni-Cu heavy alloys could only be obtained by liquid phase sintering.

Kothari [29] studied the densification and grain growth kinetics of W-Ni-Cu heavy alloys with different ratios of copper to nickel in the alloy composition. The kinetics study was carried out in the temperature range of 1200-1500°C and the sintering was carried for different periods at each temperature. The rate constant for the sintering process was evaluated from the volume change as a function of sintering period. The activation energy was found to be independent of composition. It was concluded from the grain growth kinetics data that growth rate was proportional to $t^{1/3}$ where 't' is the sintering period.

Coalescence phenomena in W-Ni-Cu alloys during liquid phase sintering were studied by Makarov *et al* [30]. Higher sintering temperature helps in better spherodization and also better properties at elevated temperature (1500°C) sintering. This may be due to less screening effect by copper around nickel particles and thus facilitating more W-Ni interactions.

Ariel *et al* [5] investigated heavy alloy of composition 90W-7Ni-3Cu from 1420-1450°C for sintering period upto 3hrs. This resulted in microstructural changes leading to changes in mean free path of tungsten grains, tungsten-matrix interfaces and the contiguity of tungsten spheroids.

Srikanth and Upadhyaya [31] carried out the effect of tungsten and copper powder size variation on the sintered properties of W-Ni-Cu heavy alloys. They showed that in the case fine tungsten at either sintering temperature of 1400°C or 1500°C, the size of the maximum occurring spheroid is larger as compared to the coarse powder based compositions. They observed the spherodization even for high nickel content in the binder at high sintering temperature. This is indicative of faster soluton-reprecipitation kinetics at the higher sintering temperature.

Ramakrishanan and Upadhyaya [32] studied the effect of composition and sintering temperature on the densification and microstructure of W-Ni-Cu heavy alloys. They found that the average grain size of tungsten particle decreases with increase in binder content and increase in sintering period. It was also concluded that the contiguity and connectivity decreases with increase in sintering period and binder content.

Kuzmic [33] proposed that rapid cooling from the sintering temperature prevent the formation of brittle phase in order to obtain good mechanical properties. Ariel *et al.* [5] correlated the mechanical properties of W-Ni-Cu system with sintered microstructure. Their study showed that the mechanical properties are a function of mean free path between tungsten grains, volume fraction of tungsten grains and the contiguity of tungsten spheroids.

2.8 Effect of Binder Content

Two factors appear to be of importance in alloys containing both copper and nickel. They are the ratio of nickel to copper and total percentage of these metals present. It has been shown that the maximum density is obtained when the nickel copper ratio is about 2 to 1, and the tungsten content is between 89 and 93 percent [28]. The optimum value of the copper-nickel ratio appears to result from two effects. The addition of copper lowers the melting point of the nickel. It ensures the presence of a liquid phase, which is able to penetrate between the tungsten grains. It reduces the solubility of tungsten in this phase. Therefore, too high a proportion of copper is a disadvantage. It should be pointed out that the optimum composition depends on the choice of sintering conditions and would be nearer the tungsten corner of the ternary diagram if the time or temperature were increased. The solubility of tungsten in binder depends on the binder composition. It is reported that nickel dissolves about 40% tungsten, whereas the solubility of nickel in tungsten is very small around 0.36% [32]. The solubility of tungsten in Cu-Ni binder increases with increase in the nickel content in the system. Srikanth and Upadhyaya [31] studied the effect of binder composition on spheroid growth of tungsten particles. They studied the effect of three binder compositions (60Cu/40Ni, 40Cu/60Ni, 20Cu/80Ni) based on the fine and coarse tungsten particles. They found that tungsten spheroid size distribution is wider with increasing nickel content in the binder. It was also found that with increasing nickel content there are two different mechanisms of spheroid growth, one is solution controlled and the other one is diffusion controlled. At higher nickel content and at high sintering sintering temperature diffusion controlled mechanism is responsible for spheroid growth.

2.9 Distortion Behavior of Tungsten Heavy Alloys:

Despite widespread application, difficulties still exist in the manufacture of liquid phase sintered tungsten heavy alloys. Compact distortion during sintering is a well-known problem in powder metallurgy. Slumping or distortion during sintering is defined as a non-isotropic shape change that accompanies densification. Large dimensional change takes place during sintering. The linear shrinkage can be as large as 20% if there is a high volume fraction of liquid present at any stage of the sintering cycle [34]. This causes slumping to occur.

The constituent liquid and solid phases seldom have the same density, therefore the heavier constituent has a natural tendency to settle, causing solid-liquid segregation and consequent distortion. In tungsten heavy alloys, the W grains and the matrix have a wide density difference (up to 9 g/cm^3). Thus, tungsten Heavy alloys are prone to distortion during liquid phase sintering. Detailed investigation of slumping in liquid phase sintered tungsten heavy alloy compacts was performed by Kipphut *et al* [35]. They concluded that gravity and density differences are responsible for settling that consequently affects distortion. Mani and German [36] treated compact distortion as a result of the gravity induced liquid flow and solid migration when there is a large amount of liquid or a high sintering temperature. They reported solid-liquid segregation in tungsten heavy alloys containing less than 83-wt.% tungsten, which led to shape loss and compositional gradients. The distortion behavior of 80W-20 (Ni, Cu) alloy was studied by Upadhyaya [37]. He found that high dihedral angle minimize compact slumping.

Chapter 3
SCOPE OF THE PRESENT WORK

In the case of heavy alloys, because of their varied applications ranging from radiation shields to counter balances, a great deal of research is devoted in their area and attempts have been made to reduce their cost. Though a number of works have been done in heavy alloys, the properties variation of these alloys with respect to variables like processing, alloy chemistry and microstructure still remains unexplained.

In the present study, we will discus the key microstructural attributes, which are responsible for determining final properties of W-Ni-Cu heavy alloy. The key microstructural attributes planned for investigation are solid content, two-dimensional and three-dimensional grain connectivity, grain contiguity, dihedral angle, surface area of W-W per unit volume, grain size, and mean free path. We also describe the alloy systems chosen for this study along with the basis for their selection.

3.1 Identification of the Key Microstructural Attributes

As it has mentioned earlier the solid content is one of the key parameters to dominate final properties of this heavy alloy. The solid content indicates the volume fraction of the solid phase in the microstructure. A high solid content results in a high packing coordination and prevents distortion.

Contiguity is a useful parameter to describe a liquid phase microstructure. It is defined as the relative fraction of the grain interface area that is solid (grain boundary). A greater structural rigidity to the compacts can be obtained through high solid-solid contiguity. Microstructural connectivity is a measure of the grain coordination numbers in two-dimension [10]. A high connectivity implies more grain-to-grain contact. Structural rigidity increases with connectivity.

The neck size is governed by the solid-liquid and solid-solid interfacial energy and is characteristic by dihedral angle. This is different from contact angle. Contact angle is three-phase interfacial energy balance (solid-liquid, liquid-vapor, and vapor-solid) phase whereas dihedral angle describes the two-phase energy balance. For a particular system, the magnitude of the ratio between the grain boundary (solid-solid) and solid-

liquid interfacial energies determines the dihedral angle. Thus, it is a measure of the degree of intergranular penetration by the liquid phase. The dihedral angle, ϕ, can be expressed as the vectorial balance of the solid-solid, γ_{SS}, and solid-liquid, γ_{SL}, interfacial energies and is given by [10]:

$$\varphi = 2Cos^{-1}\left(\frac{\gamma_{SS}}{2\gamma_{SL}}\right) = 2Sin^{-1}\left(\frac{x}{G}\right) \quad \text{.....(3.1)}$$

Where x is the intergranular neck size and G is the grain diameter. Figure 3.1 is a schematic representation of dihedral angle. A low dihedral angle system has a low solid-liquid interfacial energy. This will favor the dissolution of the intergranular necks formed by solid-state sintering during heating [10]. Consequently, the compact structural rigidity will be lost and the compact will distort.

The mean free path, λ, is the mean edge-to-edge distance between adjacent grains. It represents the average liquid film thickness separating two grains and is expressed as:

$$\lambda = \overline{G}\left[\frac{1-V_S}{V_S}\right] \quad \text{..... (3.2)}$$

Where V_S and $\overline{G}$ refer to the solid volume fraction and the average grain size. A low solid content and a large grain size result in a higher mean free path. A high liquid film thickness facilitates the grains to easily slide past each other and will make the compact more distortion prone. A high solid content results in a larger grain size.

3.2 Interrelationship between the Microstructural Attributes

The variation of contiguity with the volume fraction of tungsten heavy alloys for various dihedral angles was calculated by German [14]. He observed that the lower the dihedral angle, the smaller is the contiguity. German related the effect of various processing parameters, such as interfacial energies, grain size ratios, and solid content on the contiguity. His model suggested that the contiguity increasing with an increasing solid content and dihedral angle. However, the grain size has little influence on contiguity. German empirically related contiguity, Cg, with the solid content, Vs, and the dihedral angle as follows:

$$C_g = V_S^2\left(0.43Sin\phi + 0.35Sin^2\phi\right) \quad \text{..... (3.3)}$$

Note that a high solid content and a large dihedral angle result in a higher contiguity. These conditions should therefore result in better compact shape retention.

Usually, the three-dimensional coordination number, Nc, cannot be measured. However, it can be related to the two-dimensional grain connectivity, C_c, and the dihedral angle, ϕ as follow [38]:

$$N_C = 1.47 C_g \left(Sin \frac{\phi}{2} \right)^{-1} \quad \text{..... (3.4)}$$

The connectivity, C_g, can be experimentally measured by counting the number of grains in contact with a given central grain in a two-dimensional sectional plane. From the above equation, a high dihedral angle and high connectivity result in a large grain coordination number.

3.3 System Selection

Model experiments have been carried out on W-Ni-Cu samples. This alloy offers an ideal platform for our experiments because they attain near-full density during sintering. They have the high solid-liquid density difference (up to 9 g/cm^3). One major problem of density difference is segregation. Gravity induce precipitation may occur due to density difference. Microstructural quantification will be difficult due to these reasons. Even though there is a density difference between tungsten and binder, they are easy to process; avoid intermetallic formation during sintering and their microstructure can be varied via alloy compositions, sintering time and sintering temperature. However, there is no such density difference between copper and nickel. In addition, these alloys are well investigated and plenty of literature is available on their processing and microstructure.

Unlike W-Ni-Fe samples, the W-Ni-Cu samples give a larger solubility and dihedral angle change with composition (W content and Ni:Cu ratio). In W-Ni-Fe alloys the eutectic forms at 1435°C and the eutectic temperature depends upon binder composition and binder content. Despite these, one major problem with these alloys is formation of intermetallics. Thus, it is essential to keep nickel to iron ratio 7:3 to avoid intermetallics. The use of nickel-copper binder has large flexibility over this. There is a flexibility of changing microstructure with the same tungsten content. An increasing Ni content in the matrix reduces the dihedral angle. It also increases the solubility of

tungsten grains in the matrix. Srikanth and Upadhyaya [39] showed that an increase in the Ni content in a 90W-10 (Ni-Cu) alloy lead to larger tungsten grains and broader tungsten grain size distribution. Thus, without the changing sintering temperature, various dihedral angles can be obtained in the W-Ni-Cu system by merely changing the Ni:Cu ratio.

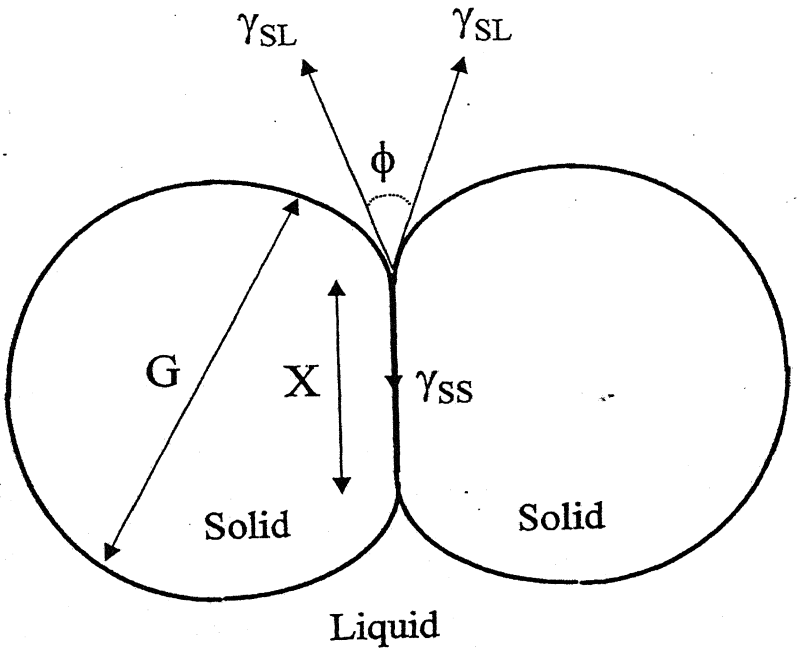

$$\phi = 2\cos^{-1}\frac{\gamma_{SS}}{2\gamma_{SL}} = 2\sin^{-1}\frac{X}{G}$$

Figure 3.1 Schematic representation of Dihedral angle [37]

Chapter 4
EXPERIMENTAL PROCEDURE

The present chapter deals with various experimental techniques used to both process and characterization the alloy. Those are a) raw materials; b) composition preparation; c) compaction; d) sintering; e) densification behavior; f) microstructural studies; g) quantitative microstructural analysis.

4.1 Raw Materials

4.1.1 Elemental Tungsten Powder

The W-powder (Grade: M55), supplied by Osram Sylvania (Towanda, PA, USA) was manufactured by reduction and had an irregular shape with the average size of 5.4 μm. with minimum and maximum size of 4.3 and 5.7 μm, respectively.

4.1.2 Elemental Copper Powder

The Cu powder (grade: 635) prepared by gas atomization was supplied by ACuPowder International (Union, NJ, USA), had a rounded shape with the average size of 13 μm in as-received condition.

4.1.3 Elemental Nickel Powder

The nickel powder (grade: 123) prepared by carbonyl process was supplied by INCO, had a spiky shape with the average size 15 μm in as-received condition.

4.2 Composition Preparation

For the investigation, the W-Ni-Cu alloys containing 80, 85 and 90-wt.% W with nickel to copper ratio 6:4, 7:3, and 8:2 were chosen. In the set of experiments, the compositions were prepared by mixing the constituents W, Cu, and Ni powders in requisite proportion. Elemental tungsten, copper and nickel were weighted to 0.0001-g accuracy using an electronic balance (supplier: Mettler, AE 200, USA). The balance was calibrated using a series of standard weights. The compositions were mixed in a Turbula mixer (type: T2C Nr. 921266, supplier: Bachofen AG, Switzerland) for 30 min. Mixing

ensures complete homogeneity in the powder mixture. To prevent segregation, adequate care should be taken that the powders were not shaken after mixing.

After the mixing of the powders to make the desire composition, the density of the W-Ni-Cu alloy was determined using the inverse rule of mixing. The theoretical density can be expressed as:

$$\frac{W}{\rho_{th}} = \frac{W_1}{\rho_1} + \frac{W_2}{\rho_2} + \frac{W_3}{\rho_3} \quad \text{..... 4.1}$$

Where, W_1, W_2 and W_3 are the weight fraction of the powders to be mixed. ρ_1, ρ_2 and ρ_3 represent their respective densities. ρ_{th} is the theoretical density of the mixture. The rule is applicable only for the non-interactive system. Table 4.2 shows the theoretical densities of various compositions.

For W-6Ni-4Cu composition,

$$\frac{1}{\rho_{th}} = \frac{0.9}{19.3} + \frac{0.06}{8.9} + \frac{0.04}{8.93} \quad \text{.....4.2}$$

$\rho_{th} = 17.287$ g/cm^3

4.3 Compaction

The powders were compacted at 200 MPa pressure using a manually operated uniaxial hydraulic press (Apex Construction Ltd., UK) of 20-t capacity. The compacts were pressed in cylindrical pellet form with diameter of 12.7 mm and height of about 4 to 6 mm. To facilitate pressing, zinc-stearate was used as die-wall lubricant. The die was made of high chromium high carbon steel was cleaned with acetone prior to each powder fill. Lubrication facilitates compaction and subsequent removal of the green compacted samples.

4.4 Sintering

Sintering of green samples was carried out in a super-Kanthal ($MoSi_2$) heated, automatic programmable, horizontal tubular furnace (model: OKAY 70T-4) supplied by Bysakh and Co., Kolkata, India. The furnace had a doubly recrystallized alumina tube with inner diameter of 7.5 cm and length 1m. The furnace had a heating zone of approximately 11 cm in the temperature range of 1400-1550°C with an accuracy of ±5°C.

The sintering was done in commercially pure hydrogen (dew point: -35°C) atmosphere. The flow rate of hydrogen was maintained at 1 l/min.

In the present work, sintering was carried out at two different temperatures, 1440 and 1460°C. Requisite number of the green cylindrical compacts were placed over an alumina boat and transferred in the heating zone of the tubular furnace. To prevent any hydrogen leakage, both ends of tubular furnace were sealed with SILASTIC (RTV 700) adhesive (sealant). Heating rates were same for all the sintering operations (5°C/min.). The samples were heated to required temperature after holding at 1000°C for 1h. This soaking was done to attain homogenization in the sample. It also provides enough time for reduction of oxide layer formed on the powder particles. Holding time was 60 min at final sintering temperature for each case. Automatic temperature controller was used to control the temperature within ± 5°C. In all cases cooling was done in hydrogen atmosphere at an average rate of 2-3°C/min to prevent oxidation during cooling. Figure 4.1 shows the sintering cycle for liquid phase sintering.

4.5 Densification Behavior (Sintered Density and Densification Parameter)

The densities of cylindrical green compacts and sintered compacts were determined through dimensional measurements. Generally, green densities of the compacts were calculated using physical dimensions and their masses. The sintered densities of distorted samples were measured by Archimedes method. An analytical balance (Mettler H31AR) was used for all the measurements. Densities were calculated by the following formula:

$$\rho_s = \frac{W_{SA}}{W_{SA} - W_{SW}} \quad \text{.....4.3}$$

Where,

ρ_s is the relative density of the sample

W_{SA} is the weight of the sample in air

W_{SW} is the weight of the sample in the water

Table 4.1 Experimental Details

Alloys	Tungsten	Ni:Cu	Composition
W-Ni-Cu	80 wt%	6:4	W-12Ni-8Cu
		7:3	W-14Ni-6Cu
		8:2	W-16Ni-4Cu
	85 wt%	6:4	W-9Ni-6Cu
		7:3	W-10.5Ni-4.5Cu
		8:2	W-12Ni-3Cu
	90 wt%	6:4	W-6Ni-4Cu
		7:3	W-7Ni-3Cu
		8:2	W-8Ni-2Cu

Table 4.2 Theoretical densities of various compositions.

Composition, (wt.%)	Theoretical Density, ρ_{th}, g/cm^3
90W-6Ni-4Cu	17.287
90W-7Ni-3Cu	17.286
90W-8Ni-2Cu	17.284
85W-9Ni-6Cu	16.430
85W-10.5Ni-4.5Cu	16.428
85W-12Ni-3Cu	16.427
80W-12Ni-8Cu	15.654
80W-14Ni-6Cu	15.652
80W-16Ni-4Cu	15.650

Theoretical densities of elemental tungsten, nickel, and copper powders are given below-

Tungsten (W) = 19.3 g/cm^3

Nickel (Ni) = 8.904 g/cm^3

Copper (Cu) = 8.934 g/cm^3

Sintering Cycle

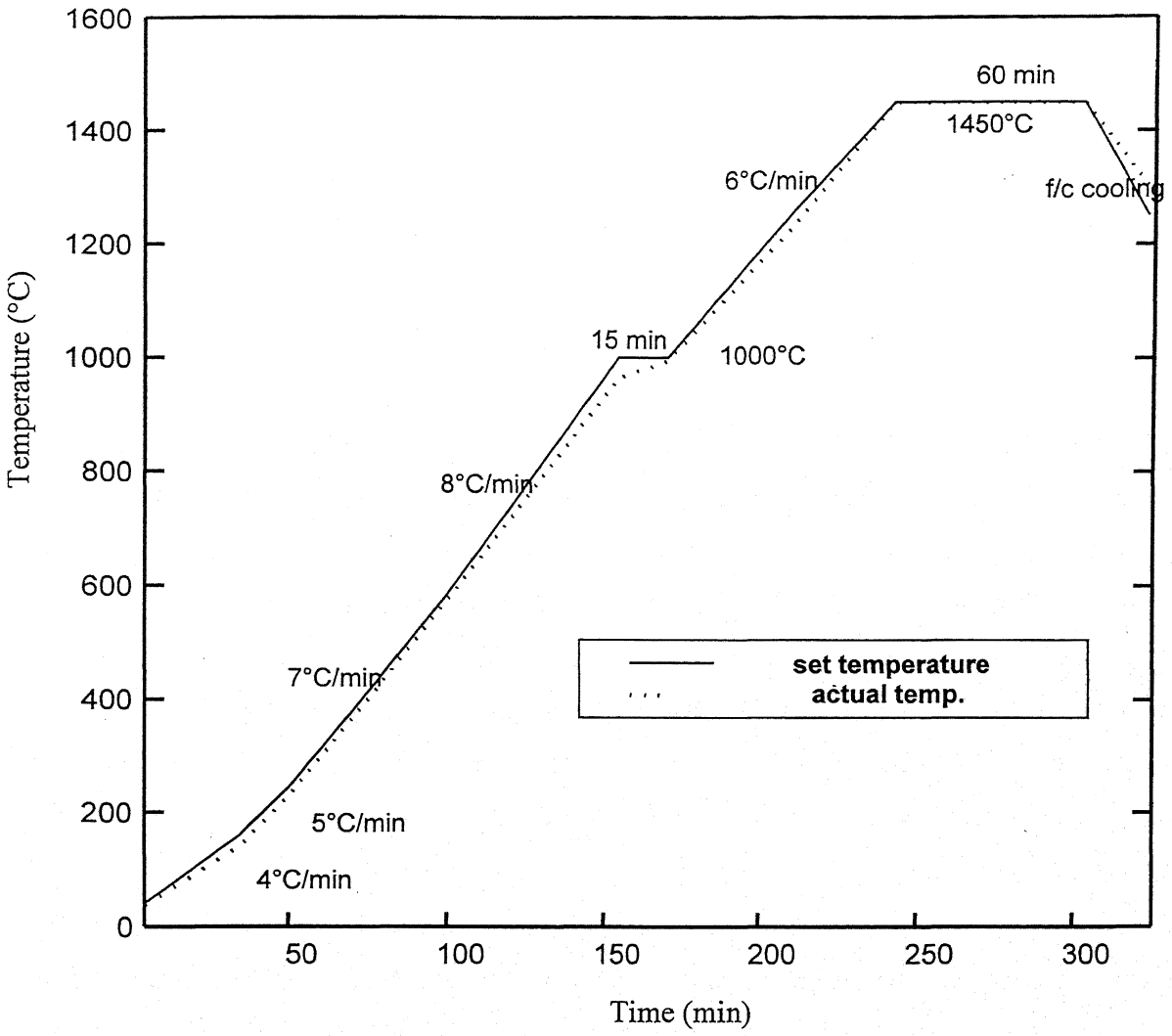

Figure 4.1. shows Sintering cycle for the W-Ni-Cu alloys

Densification parameter was also a way to determine the amount of densification occurred after sintering. Densification parameter (ψ) was expressed as follows-

$$\psi = \frac{SD - GD}{TD - GD} \quad \text{.....4.4}$$

Where,

SD is the sintered density,

GD is the green density,

TD is the theoretical density.

Theoretical densities of various compositions were determined by inverse rule of mixing, taking the theoretical densities of various elements at room temperature.

4.6 Quantitative Metallography

4.6.1 Specimen Preparation

All the sintered distorted samples were sectioned longitudinally to get flat surface. This was followed by cold mounting. Care was taken while mounting in order to maintain good gripping of samples with in the mount and flatness of samples. Grinding was the next step that includes considerable relief in the matrix or results in a dual plane structure. In other words, the two phases of the material being processed will be on two different levels. It also helps in proper flattening of the samples and making polishing further easier. All the sintered compacts were polished manually on a 'Lunn Major Polisher of Struers make, Denmark' having four grades of emery papers 1/0, 2/0, 3/0 and 4/0 in that order, followed by fine wheel polishing with suspended 0.03 μm size alumina in distilled water. This is attributed to the fact that the emery paper used quickly grinds away the soft Cu-Ni matrix while leaving the hard tungsten particle untouched. Hence, emery papers were only used for primary removal of scratches.

4.6.2 Microstructural Studies

Tungsten heavy alloys have good contrast in micrographs without etching. Therefore, all the optical micrographs were taken in unetched condition by LEICA@500IW image analyzer. The volume fraction of solid, contiguity, connectivity, interfacial area of tungsten-matrix per unit volume, mean dihedral angle and average tungsten spheroid size

were characterized manually through microstructural analysis with the help of LEICA@500IW image analyzer.

4.6.2.1 Volume fraction of Solid

In quantitative metallography, systematic point count analysis was carried out to evaluate the volume fraction of solid particles of as-received samples containing 80 to 90, wt.% W. In systematic point count analysis, a square grid with 30 grid points as shown in Figure 4.2, was superimposed on the microstructure. The number of grid points falling on the particles were counted systematically and compared with total number of grid points. If total number of grid points falling on the phase of interest is P_i and total number of grid points is P_a, then the point fraction P_p is given by-

$$P_p = \frac{P_i}{P_a} \quad \text{.....4.5}$$

It will give the volume fraction (V_v) of the particle. The advantage of using the systematic point count analysis is that the relative error is low (10%) as compared to other methods available. The same procedure was carried out on 30 fields of views of the same sample, and mean was considered as final result.

4.6.2.2 Contiguity of the Microstructural Surface

Contiguity is a measure of solid-solid contact in the liquid phase sintered material [38] and it is given mathematically as-

$$C_g = \frac{2p_L^{w/w}}{2p_L^{w/w} + P^{w/m}} \quad \text{.....4.6}$$

Where the C_g = Contiguity of the micro structural surfaces

$p_L^{w/w}$ = Number of intercepts made by solid-solid contact per unit length of test line.

$p_L^{w/m}$ = Number of intercepts made by solid-matrix contact per unit length of test line.

Contiguity would vary between 0 and 1. A value of '0'indicates that there is no solid contact and a value of '1' implies 100% contiguous structure. The same calculation was done on thirty fields of view of a particular sample. The mean value was taken as

contiguity factor of that sample. Figure 4.3 shows the contiguity measurement on microstructure.

4.6.2.3. Connectivity

Connectivity is the number of grain-grain contacts per grain. It is the two dimensional grain coordination between grains in a liquid phase microstructure [39]. It is a measure of rigidity of the microstructure. It has a positive correlation with contiguity. It increases whenever contiguity increases and vice-versa. The grain connectivity was measured by counting the number of grains mutually in contact with a given central grain. The connectivity measurement was done on about 200 grains per sample. The mean value was reported.

4.6.2.4. Surface Area per unit Volume (S_v)

Surface area per unit volume of the W-W and W-Matrix interfaces were calculated using five lines of equal length. The total number of points of intersections with the solid-solid (W-W) contact and solid-liquid (W-matrix) was calculated for 30 fields of views shown in Figure 4.3. Finally, this produced the points per unit length (P_L). Then (S_v) was calculated as

$$S_v = 2\,P_L \quad \text{.....4.7}$$

Where L = Length of line in terms of μm varies depending upon the magnification.

4.6.2.5. Mean Grain Size

The grain size was calculated from volume fraction (Vv) and surface area per unit volume of the W-W amd W-Matrix interface. Grain size varies with respect to surface area per unit volume of the particle. The mean grain size is related to V_v and S_v discussed below-

$$V_v^{(w)} = L_L^{(w)} = \frac{\sum l_i}{L} = \frac{n\sum l_i}{nL} = \frac{n\bar{l}}{L}$$

n = no. of tungsten grains intersected

$$m = n + n_m = N_{w/w} + N_{w/m}$$

$$\text{Now, } n_m = \frac{N_{w/m}}{2}$$

$$\text{Therefore, } n + \frac{N_{w/m}}{2} = N_{w/w} + N_{w/m}$$

$$n = N_{w/w} + \frac{1}{2} N_{w/m}$$

$$V_v^{(w)} = \frac{(N_{w/w} + \frac{N_{w/m}}{2})\bar{l}}{L}$$

$$V_v^{(w)} = \left(\frac{N_{w/w}}{L} + \frac{N_{w/m}}{2L} \right) \bar{l}$$

$$= (P_L^{w/w} + \frac{P_L^{w/m}}{2})\bar{l}$$

$$= \left(\frac{S_v^{w/w}}{2} + \frac{S_v^{w/m}}{4} \right) \bar{l}$$

$$\bar{l} = \frac{4V_v^{(w)}}{2S_v^{w/w} + S_v^{w/m}} \quad \text{.....4.8}$$

Where,

V_v^w = Volume fraction of tungsten particle

$S_v^{w/w}$ = Surface area of W-W interface per unit volume

$S_v^{w/m}$ = Surface area of W-Matrix interface per unit volume

4.6.2.6 Dihedral Angle

. The dihedral angle is the angle between the two contacting solid-solid grains. It provides the balance between solid-solid and solid liquid interfacial energy. Absolute measurement of interfacial energy is quite difficult. The dihedral angle cannot be measured directly on two-dimensional micrographs. However, Riegger and Van Vlack showed that the mean dihedral angle as measured on two-dimensional sections is the best estimate of the true value [40]. Sangal [41] applied stereology for the estimation of dihedral angle distribution in polycrystals. He developed two methodologies for the estimation of the distribution of true dihedral angle from a distribution of plane dihedral angle (i.e. angles between grain boundary segments in a poly crystalline microstructure).

The dihedral angle measurement was performed by manually measuring the angle between two connecting grains using a protractor [40]. A dihedral angle is shown in Figure 4.4. The measured angles are distributed over a range. The median of the distribution of the angles was selected to represent the average dihedral angle [42]. About 200 measurements on each specimen were performed. These measurements were reported by an automated image analysis technique developed by Chhabra *et al* [43] and Chhillar [44]. The technique is briefly discussed in the next section.

4.7 Automated Measurement of Dihedral Angle

In the present study, a unique methodology has been developed to determine dihedral angle of polycrystalline two-phase microstructure automatically. This method is divided into 3 steps-

a) Image Processing Algorithm
b) Neck point detection
c) Evaluation of Plane Dihedral Angle

Figure 4.5 shows microstructure of a W-Ni-Cu liquid phase sintered alloy. The marked region has been used for showing the further processing steps. Figure 4.6 shows the marked region separately. A typical binarized image of the microstructure of WHA and the corresponding bimodal gray level distribution are shown in figures 4.7a and 4.7b respectively. For the binarization of such images, automatic thresholding was applied [43]. This type of binarization gave consistent results independent of image contrast and brightness. Figure 4.7c shows the resulting binary images in which the entire sensor noises and background illumination variation have been abstracted. This binarized image was further processed by applying the erosion, thinning and pruning filters that resulted in the final processed image. Figure 4.8a shows the final processed image and 4.8b and 4.8c shows the kernels used for thinning and pruning respectively. The final image was converted into a bitmap. Figure 4.9a shows a bitmap of the rectangular region marked in figure 4.6 and figure 4.9b of the corresponding region in unprocessed image. As can be seen from this figure, the grain boundary pixels are represented by 0's and the matrix pixels are represented by 1's (these pixels uniquely had a value of 255 in the binary

image). The bitmap was used, as input to the algorithm developed to detect the necks and determine their geometry, as discussed below.

Uniqueness of the approach lies in the fact that both processed and unprocessed image bitmaps are used by the algorithm for producing results. This very unique feature of the approach is used to get much more accurate results when compared with the results obtained using only the processed image. As can be seen from the comparison between figure 4.7c and figure 4.8, neck point in the unprocessed binarized image appears very clearly as the intersection of the two grain-boundaries but in the final processed image, neck appears as a smooth curve and not as a single point. This loss of information in the image takes place during the processing of the image and it results in erroneous calculations. It is to solve this problem of information loss during processing that both the images are used simultaneously. First the processed image bitmap was used for initial identification of necks by the procedure mentioned below.

Each grain boundary pixel (pixel value of '0') was considered at the center of a 3x3 matrix. If a grain boundary pixel had exactly two other boundary pixels in its neighborhood then the pixel is a part of a grain boundary. Any point having more then 2 surrounding pixels is rejected. After identifying each such pixel of the grain boundary they were checked for the inversion where the criteria is to check for the angle between the two line segments that emerge from that point in either direction and if that value is less then a certain predefined minimum angle (which can be decided suitably for the sample, in our case its almost always less then 120 degrees) then the point is taken as an inversion point. If the angle criterion is satisfied by more than one pixel in the immediate surroundings then the one with minimum angle is considered as the inversion point. This initial angle measurement is done without any curve fitting. Five grain-boundary pixels are considered on each side of the point and the slopes are calculated on these segments by assuming them as straight lines. On satisfying the initial criterion, the pixel is subjected to more precise angle measurement.

Using this inversion point, grain boundary pixels are traced in either direction to some finite maximum distance. But as mentioned above, these pixels lack in complete information of the microstructure, so the corresponding grain boundary pixels from the unprocessed image are now detected by using these pixels from the processed image.

These pixels from the unprocessed image are next subjected to an algorithm, which does curve fitting and dihedral angle measurement on them. Further details about this work can be found in the work done by Chhabra *et al.* [43] and Chhillar [44].

4.8 Mechanical Properties

Bulk hardness and micro-hardness were measured to quantify the mechanical properties of W-Ni-Cu alloys.

4.8.1 Bulk Hardness

LECO V-100-C1 Vicker Hardness Tester at 0.5-kg load was used to measure bulk hardness values of sintered compacts. The load was applied for 15 s. A diamond pyramid indenter was used to get a square shaped indentation. The indentation was observed under attached microscope. The length of diagonal of the square indentation was measured. The Vicker Hardness (HV) values were calculated automatically by the tester itself. Five indentations were done for each sintered compact and the average value has been reported.

4.8.2 Micro-Hardness

Micro-hardness of sintered compacts was measured by Leitz 8299 micro-hardness tester. The hardness was measured on tungsten particles and matrix phase. The load used for indentation was 5 g and 50 g for matrix and tungsten spheroid respectively. The load was applied for 15 s. The indentation was square shaped. A scale attached on the microscope measured diagonal length of the square. Hardness was obtained directly from the chart given in the manual for corresponding load and diagonal length. Five indentations were taken for each sample and the average value was reported.

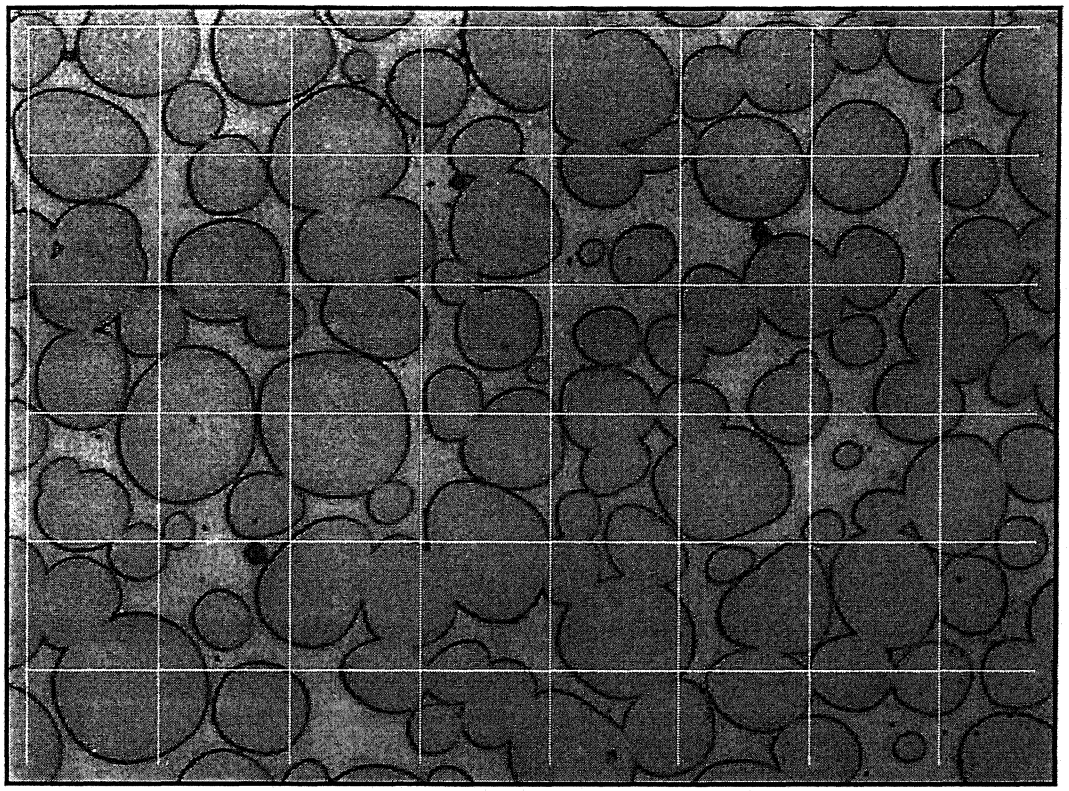

Figure 4.2: Superimposing grid on a Micrograph for calculation of volume fraction of particular phase

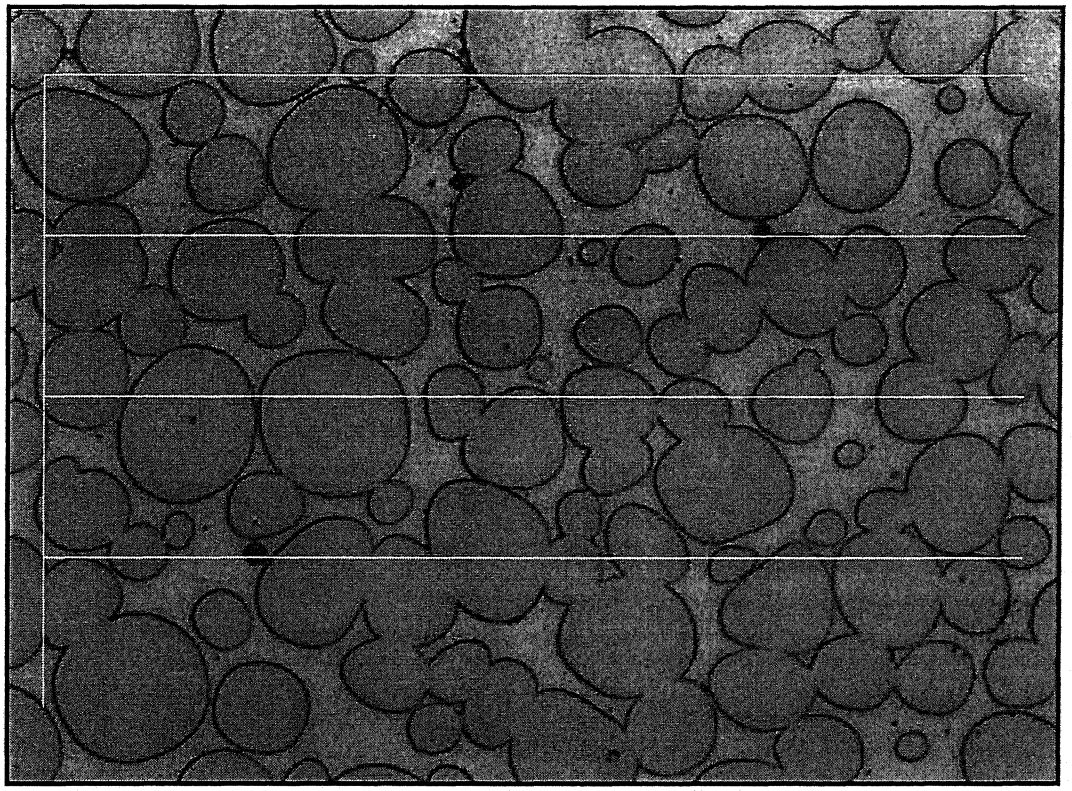

Figure 4.3: Measurement of Contiguity.

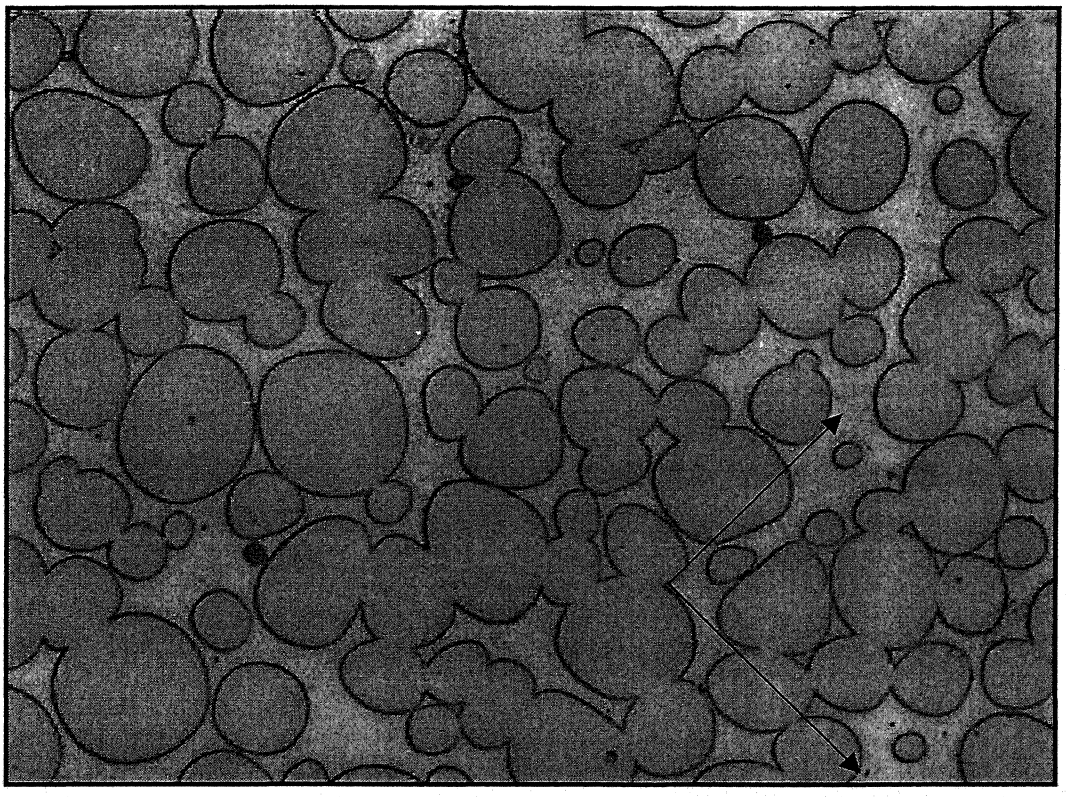

Figure 4.4. Manual Measurement of Dihedral Angle

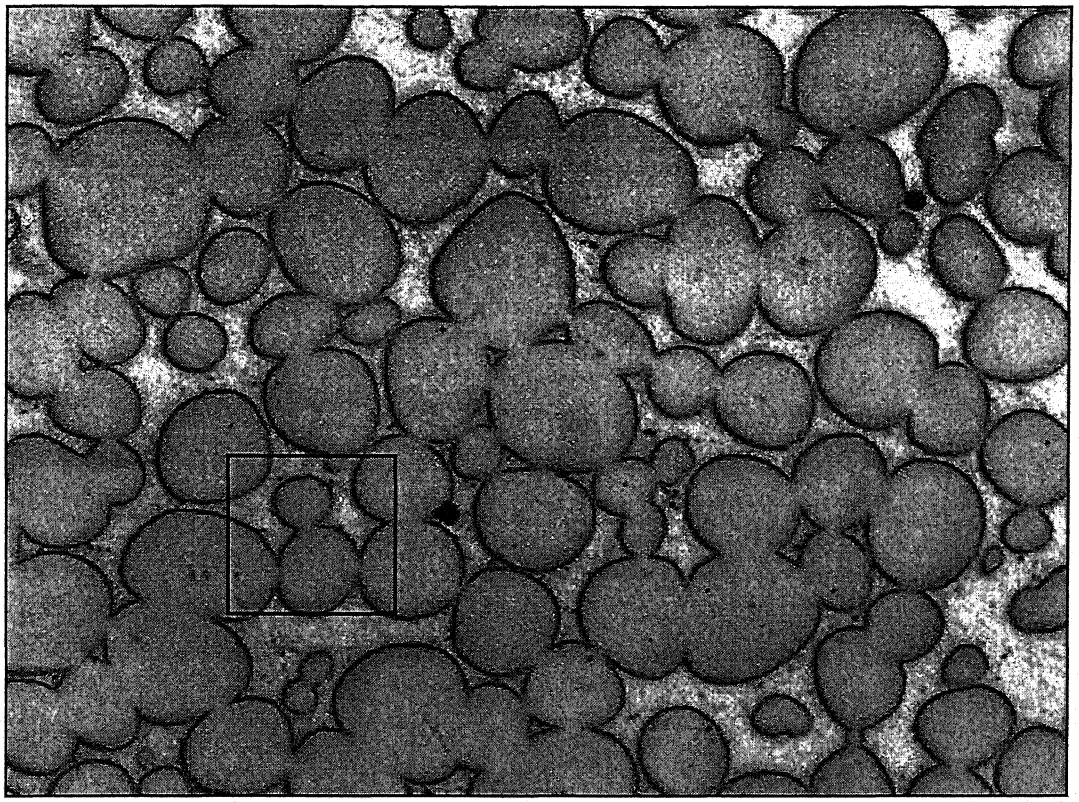

Figure 4.5: Microstructure of a W-Ni-Cu liquid phase sintered alloy. The marked region has been used for showing the further processing steps.

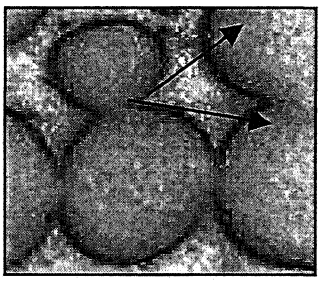

Figure 4.6: Marked region from figure 4.5, shown here is the dihedral angle.

(a)

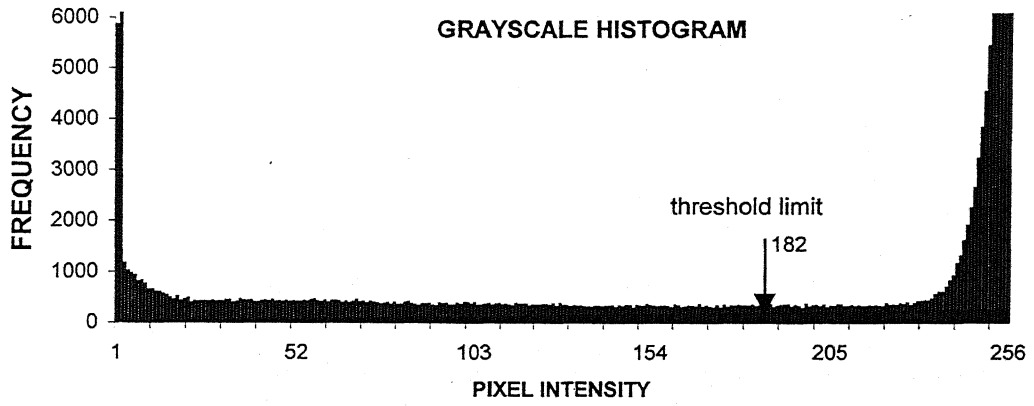

(b)

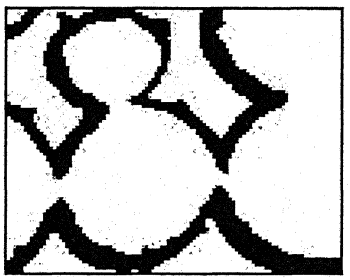

(c)

Figure 4.7: (a) A typical grayscale image of a polycrystalline microstructure; (b) Bimodal gray level histogram of the image in figure (a), arrow mark indicates thresholding limit; (c) transformed binary image after applying thresholding algorithm.

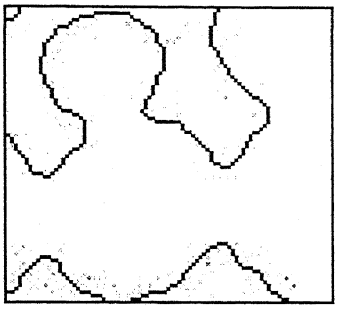

(a)

1	1	1
X	0	X
0	0	0

(b)

1	0	1
1	1	1

(c)

Figure 4.8: (a) fully processed image, (b) Kernel for thinning and (c) kernel for pruning

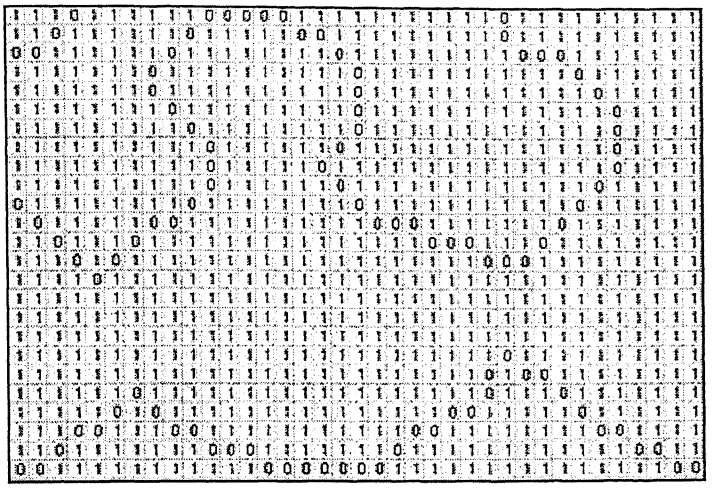

(a)

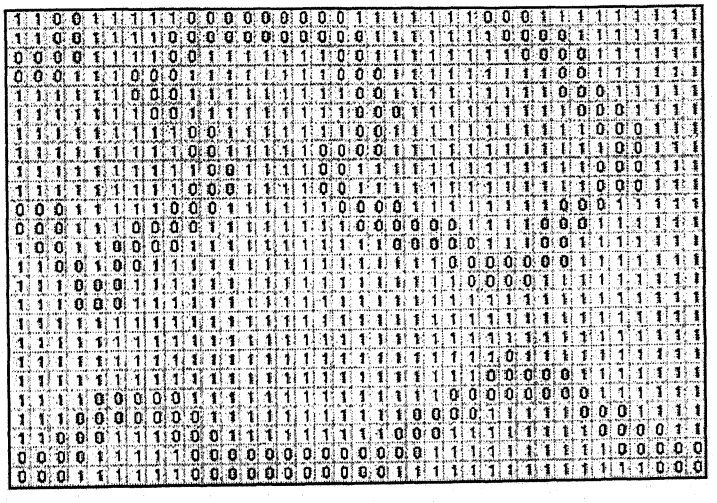

(b)

Figure 4.9: (a) Bitmap of the processed image and (b) bitmap of the unprocessed image.

Chapter 5
EXPERIMENTAL RESULTS

The experimental results of the present investigation are described in this chapter. Liquid phase sintering of compacts made from mixed powders is a low cost fabrication route. However, to achieve require properties of heavy alloys for various application needs an understanding of the relationships between processing, microstructure and properties. These links are experimentally investigated for the W-Ni-Cu system.

5.1 Densification Behavior

As described in the earlier chapters, the present study has been carried out in premixed route. It means that the compositions were prepared by mechanically mixing the elemental W, Ni, and Cu powders in requisite proportion. Figures 5.1a and 5.1b show the sintered density, % theoretical and densification parameter variation in 80W, 85W and 90W alloys with different Ni to Cu ratio sintered at 1360°C respectively. It was observed that both sintered density and densification parameter are less in compacts having 90wt%. W compared to others. Densification of compacts increases as the nickel content decreases in the system.

Figure 5.2a and 5.2b depict the densification parameter variation in 80W, 85W and 90W alloys with different Ni to Cu ratio sintered at 1440°C and 1460°C. Densification graphs show that the densification is much in 90W samples.

Figure 5.3a and 5.3b depict the % theoretical sintered density variation in 80W, 85W and 90W alloys with different Ni to Cu ratio sintered at 1440°C and 1460°C. It has been observed that densification in samples having 6:4 and 8:2 Ni to Cu ratio is more than samples having 7:3 Ni to Cu ratio. Higher densification was observed in case of compacts having 90 wt.% tungsten. There was no such huge difference in densification with respect to slight increase in temperature.

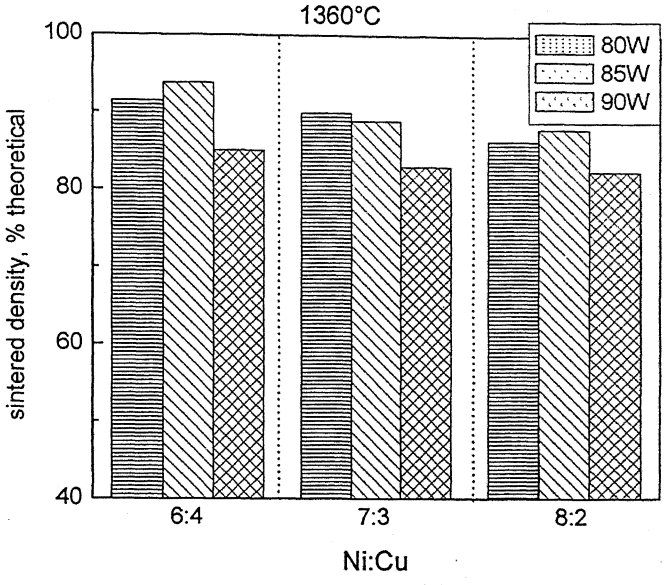

(a)

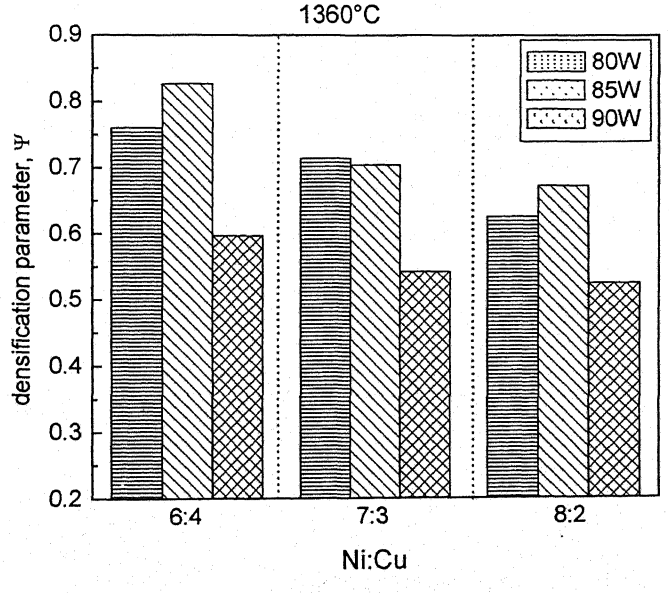

(b)

Figure 5.1. Effect of Nickel to Copper ratio on (a) sintered density and (b) densification parameter of W-Ni-Cu alloys, sintered at 1360°C.

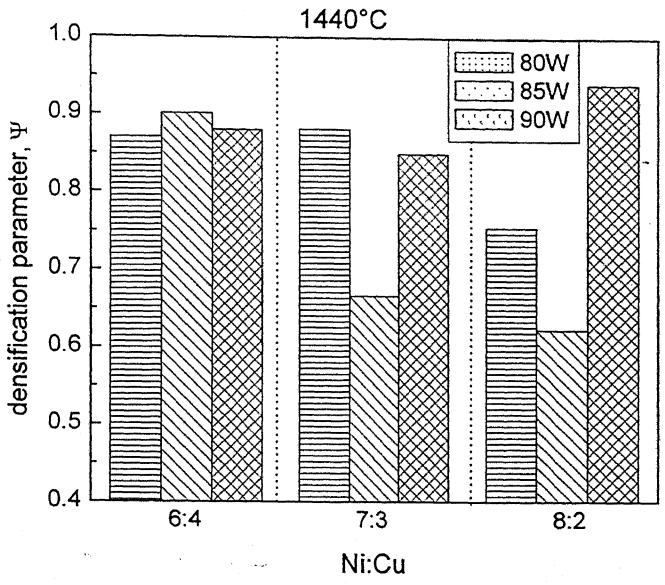

(a)

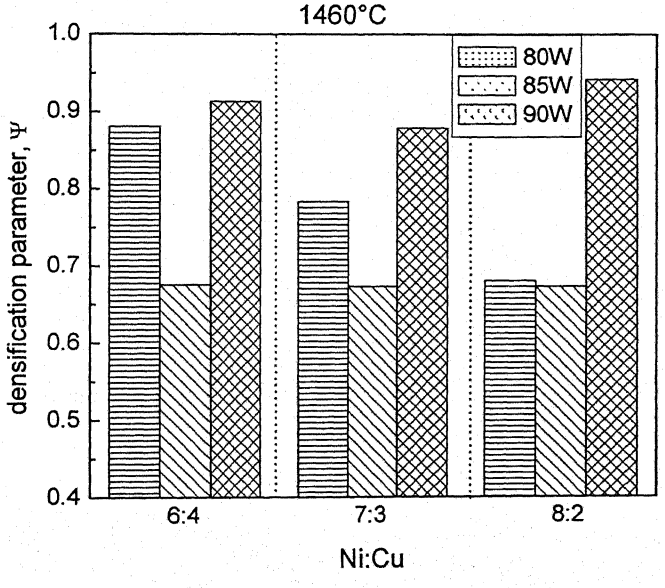

(b)

Figure 5.2. Effect of Nickel to Copper ratio on densification parameter of W-Ni-Cu alloys, sintered at (a) 1440°C and (b) 1460°C.

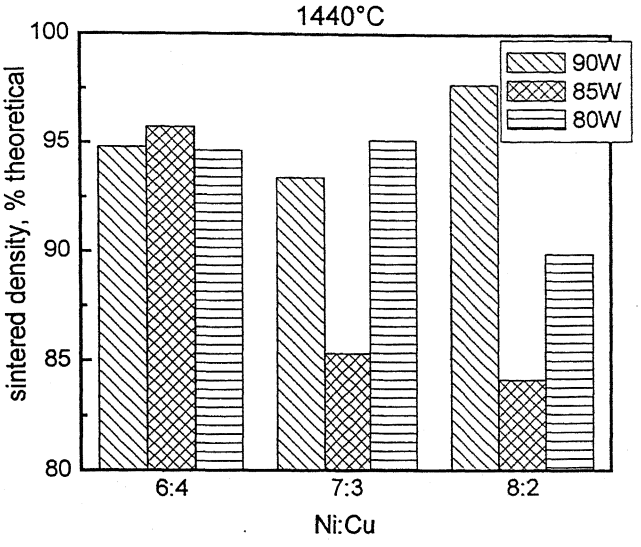

(a)

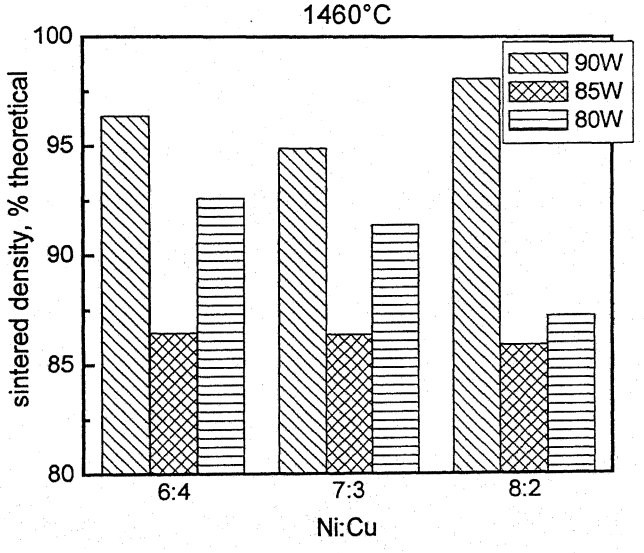

(b)

Figure 5.3. Effect of Nickel to Copper ratio on sintered density of W-Ni-Cu alloys, sintered at (a) 1440°C and (b) 1460°C.

5.2 Microstructure Evolution

The tungsten heavy alloys are generally processed by liquid phase sintering. The microstructure generally consists of spheroid tungsten grains embedded in binder matrix. Heavy alloys can be consolidated through solid-state sintering. Solid-state sintering does not provide full density.

Figures 5.4 to 5.6 show the solid-state sintered microstructures of W-Ni-Cu alloys. Figures 5.4a to 5.4c represent the microstructure of 80W-20(Ni-Cu) alloys sintered at 1360°C containing 6:4, 7:3 and 8:2 Ni to Cu ratio respectively. It was observed that small amount of liquid pool surrounds the tungsten skeleton. Figures 5.5a to 5.5c depict the microstructures of 85W-15(Ni-Cu) alloys sintered at 1360°C containing 6:4, 7:3 and 8:2 Ni to Cu ratio respectively. It was observed that amount of matrix reduces with increasing tungsten content in the system. Figures 5.6a to 5.6c show the micrographs of 90W-10(Ni-Cu) alloys sintered at 1360°C containing 6:4, 7:3 and 8:2 Ni to Cu ratio respectively. It has been seen that solid-state sintering is responsible for more porous structure. The amount of tungsten content determines the amount of matrix in the microstructure, which is clearly noticed in the above-mentioned micrographs.

Figures 5.7a to 5.7c represent the microstructure of 80W-20(Ni-Cu) alloys sintered at 1440°C containing 6:4, 7:3 and 8:2 Ni to Cu ratio respectively. It was observed that grain rounding is prominent in lower nickel content. The microstructures all are homogeneous. The sintered sample having nickel to copper ratio 8:2 depicts under sintered microstructure.

Figures 5.8a. to 5.8c show the microstructures of 80W-20(Ni-Cu) alloys sintered at 1460°C containing 6:4, 7:3 and 8:2 Ni to Cu ratio respectively. The higher sintering temperature leads to grain growth. In all alloys the tungsten grain size increases with increasing sintering temperature. Coalescence phenomena is prominent in higher matrix content. The tungsten spheroids are special characteristic features of these microstructures. It was observed that matrix volume fraction increases with nickel content.

Figures 5.9a to 5.9c depict the microstructures of 85W-15(Ni-Cu) alloys sintered at 1440°C containing 6:4, 7:3 and 8:2 Ni to Cu ratio respectively. These show the same trend as it was observed in case of Figures 5.8. The basic difference is in solid content.

The samples having higher amount of tungsten content show higher solid content in the microstructures.

Figures 5.10a to 5.10c show the micrographs of 85W-15(Ni-Cu) alloys sintered at 1460°C containing 6:4, 7:3 and 8:2 Ni to Cu ratio respectively. It was observed that grain growth takes place at higher sintering temperature. It leads to higher sintered density. At higher nickel content, the dissolution of tungsten into matrix phase is prominent in these microstructures.

Figures 5.11a to 5.11c show the micrographs of 90W-10(Ni-Cu) alloys sintered at 1440°C containing 6:4, 7:3 and 8:2 Ni to Cu ratio respectively. It has been noticed that more contiguous structure can be obtained by increasing tungsten content in the compact. Liquid pool was observed in sample having nickel to copper ratio 8:2.

Figures 5.12a to 5.12c show the microstructures of heavy alloys containing 90 wt.% tungsten, sintered at 1460°C containing 6:4, 7:3 and 8:2 Ni to Cu ratio respectively. From the microstructures, better densification is confirmed. It can be seen that there is a decrease in average grain size of the tungsten particles with increase in nickel content in the binder phase.

(a)

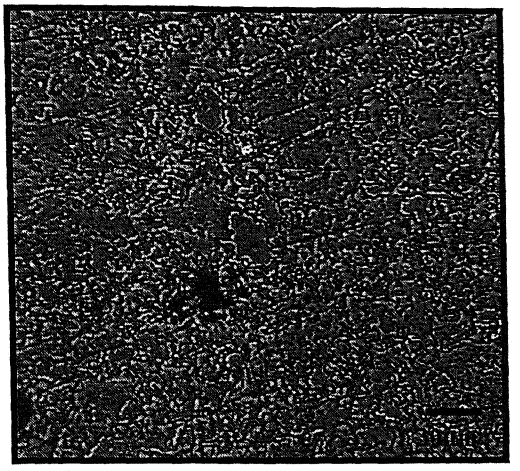

(b)

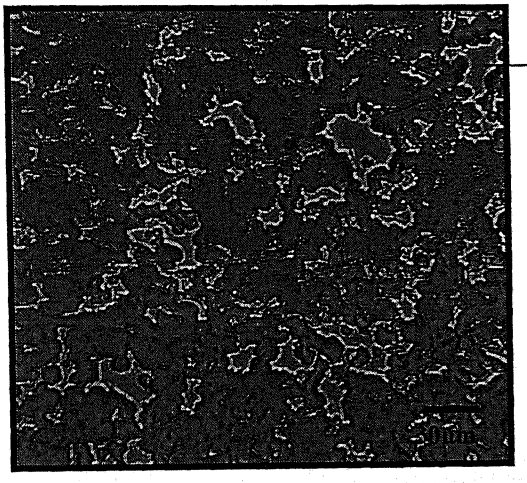

(c)

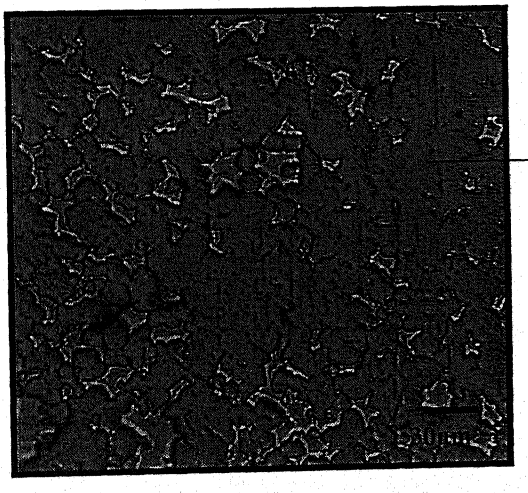

Figure 5.4. Optical Micrographs of 80W-20(Ni-Cu) sintered at 1360°C with nickel to copper ratio (a) 6:4, (b) 7:3, (c) 8:2.

(a)

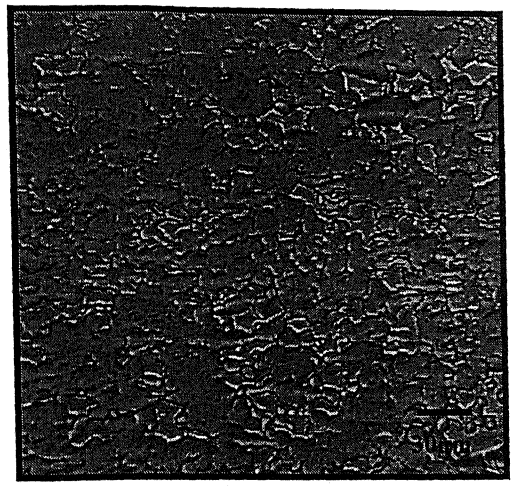

(b)

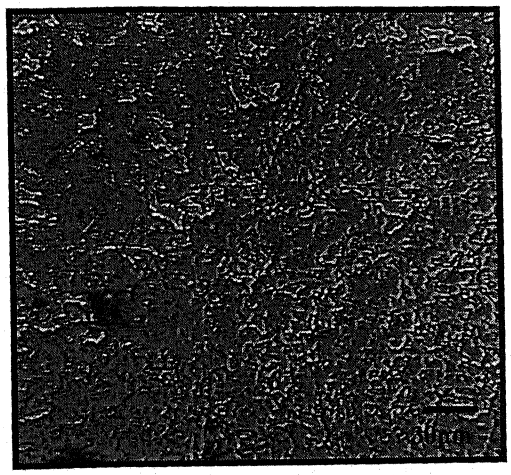

(c)

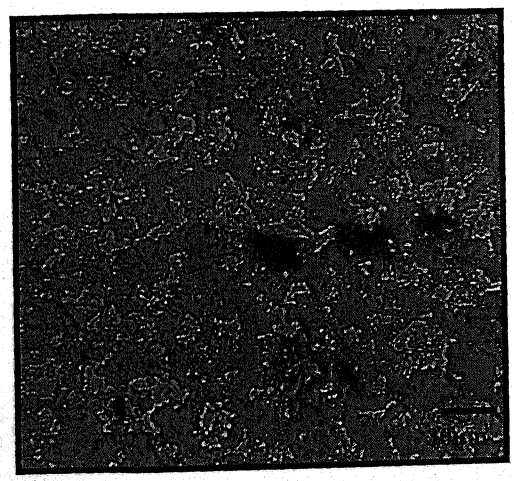

Figure 5.5. Optical Micrographs of 85W-15(Ni-Cu) sintered at 1360°C with nickel to copper ratio (a) 6:4, (b) 7:3, (c) 8:2.

(a)

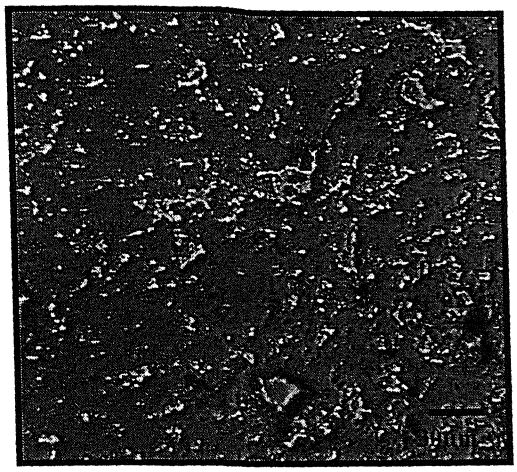

(b)

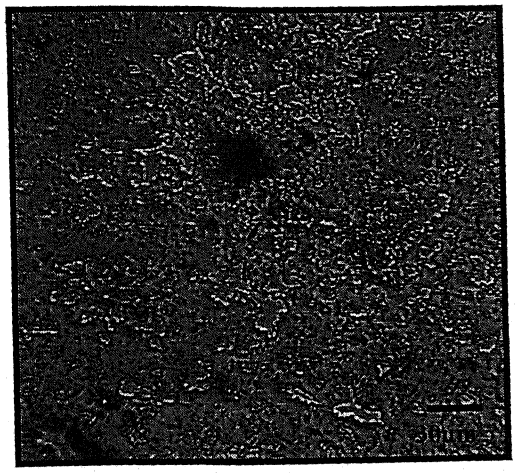

(c)

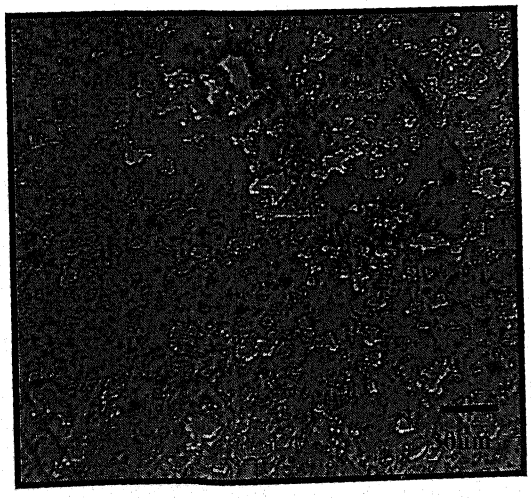

Figure 5.6. Optical Micrographs of 90W-10(Ni-Cu) sintered at 1360°C with nickel to copper ratio (a) 6:4, (b) 7:3, (c) 8:2.

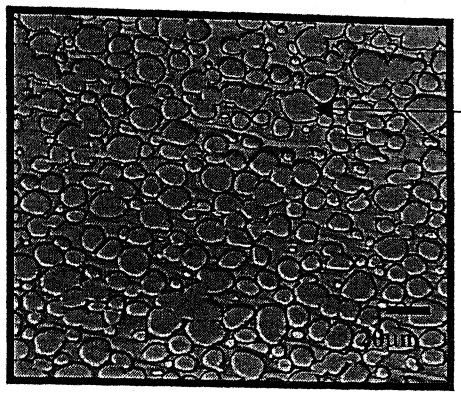

(a)

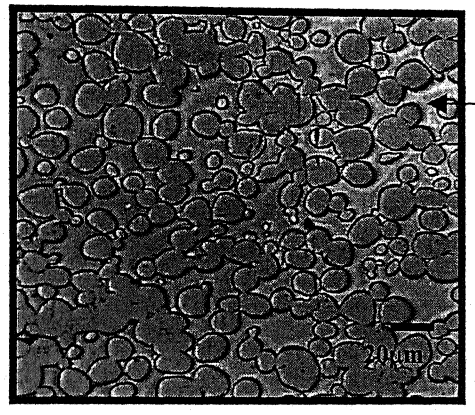

(b)

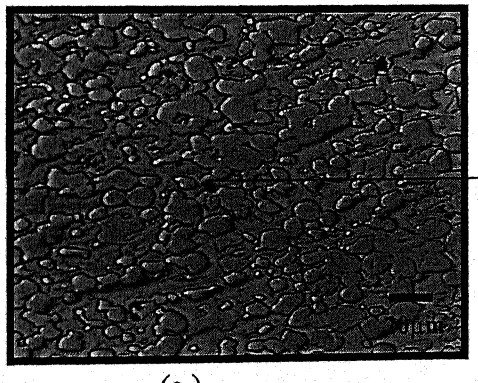

(c)

Figure 5.7. Optical Micrographs of 80W-20(Ni-Cu) sintered at 1440°C with nickel to copper ratio (a) 6:4, (b) 7:3, (c) 8:2.

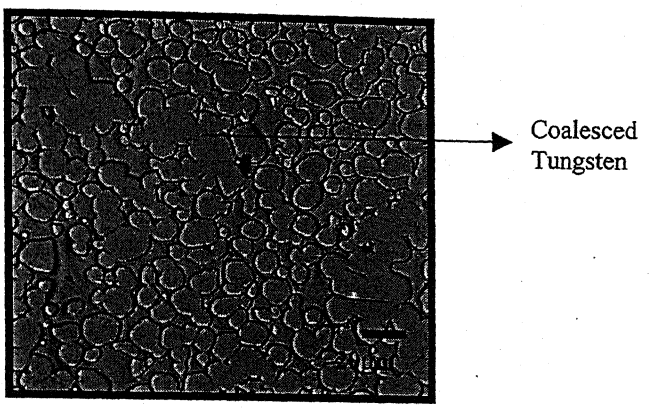

(a)

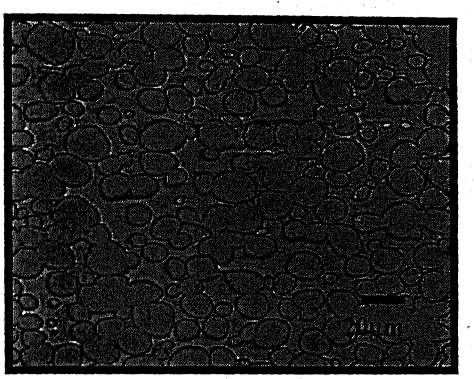

(b)

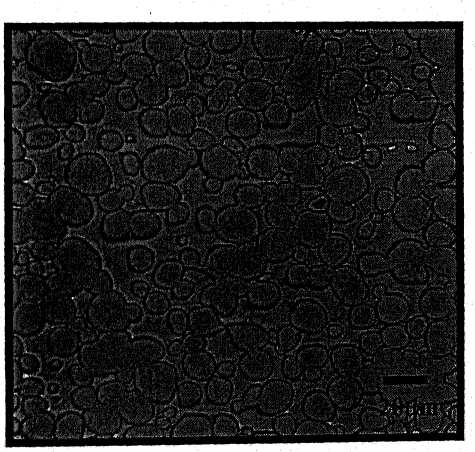

(c)

Figure 5.8. Optical Micrographs of 80W-20(Ni-Cu) sintered at 1460°C with nickel to copper ratio (a) 6:4, (b) 7:3, (c) 8:2.

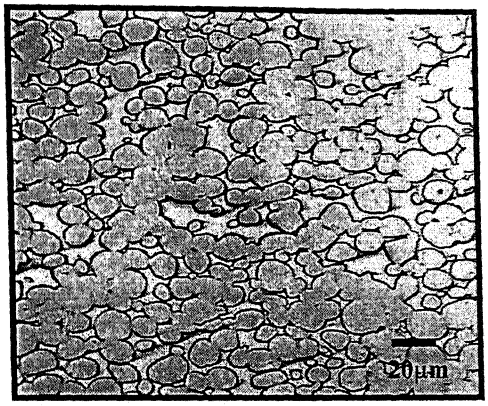

(a)

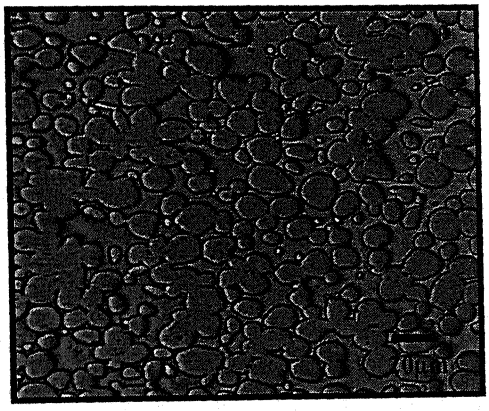

(b)

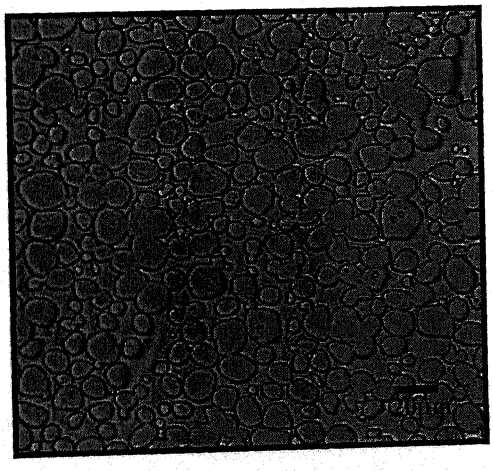

(c)

Figure 5.9. Optical Micrographs of 85W-15(Ni-Cu) sintered at 1440°C with nickel to copper ratio (a) 6:4, (b) 7:3, (c) 8:2.

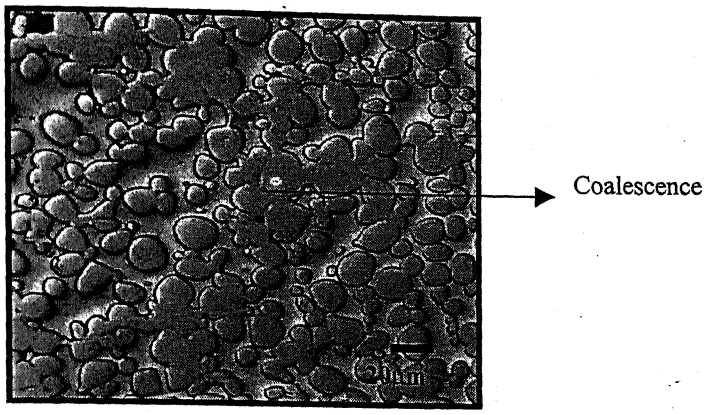

(a)

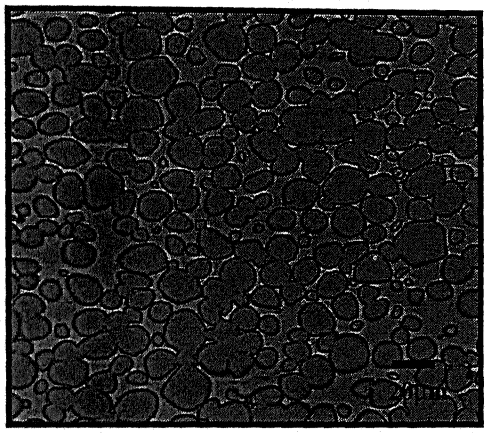

(b)

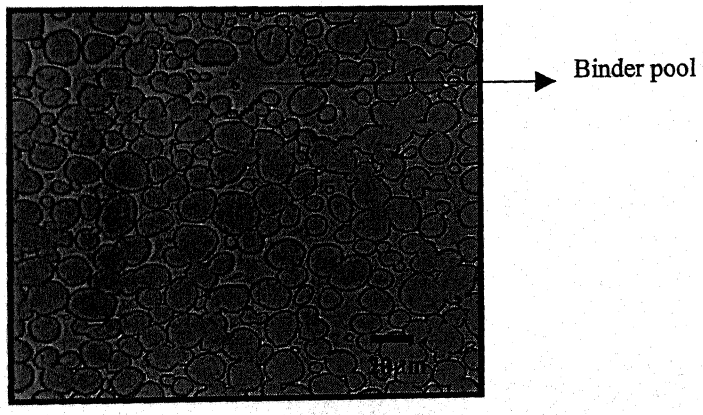

(c)

Figure 5.10. Optical Micrographs of 85W-15(Ni-Cu) sintered at 1460°C with nickel to copper ratio (a) 6:4, (b) 7:3, (c) 8:2.

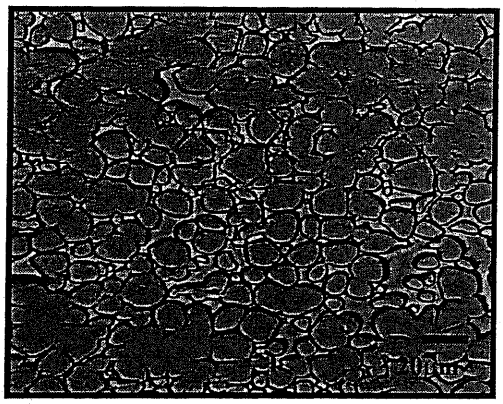

(a)

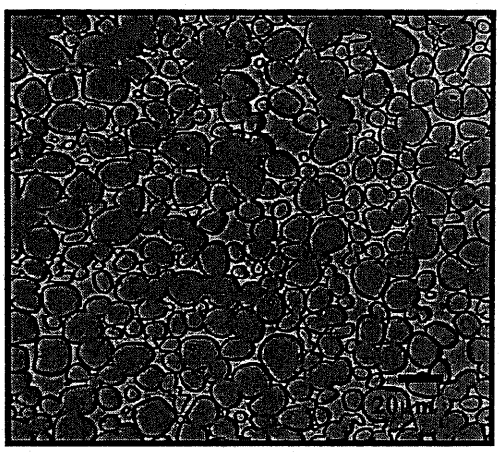

(b)

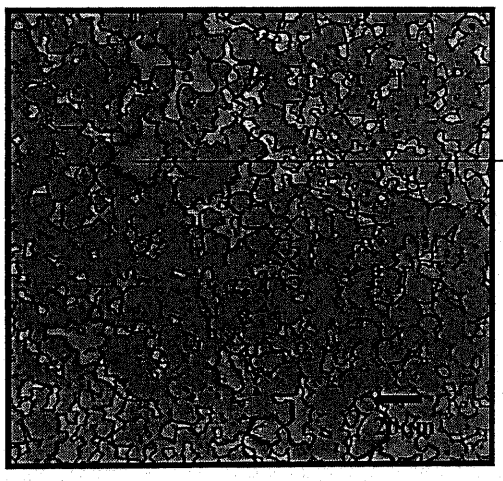

(c)

Figure 5.11. Optical Micrographs of 90W-10(Ni-Cu) sintered at 1440°C with nickel to copper ratio (a) 6:4, (b) 7:3, (c) 8:2.

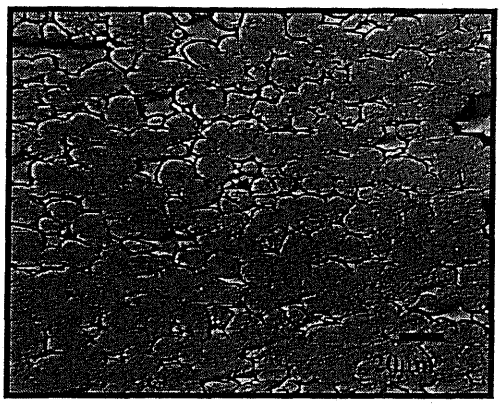

(a)

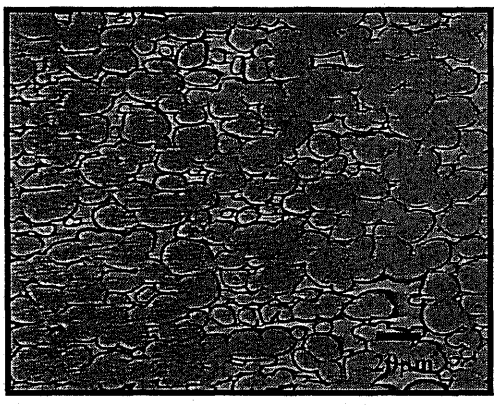

(b)

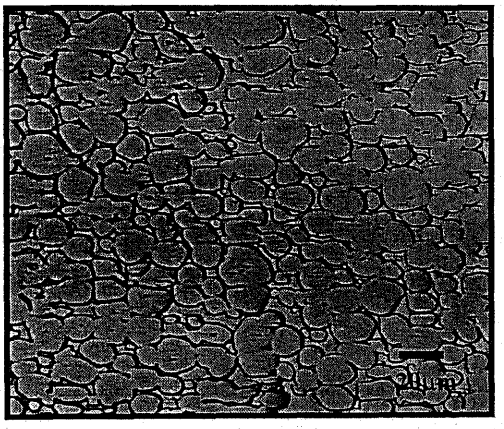

(c)

Figure 5.12. Optical Micrographs of 90W-10(Ni-Cu) sintered at 1460°C with nickel to copper ratio (a) 6:4, (b) 7:3, (c) 8:2.

5.3 Quantitative Metallography

In this section, we will discuss the following quantitative parameters such as-

5.3.1 Volume Fraction of Solid

Figures 5.13a and 5.13b show the effect of Ni to Cu ratio on volume fraction of solid of 80W, 85W and 90W alloys sintered at 1440°C and 1460°C respectively. It was observed that volume fraction of solid increases as the amount of tungsten in the system increases. It decreases with increasing amount of nickel in the system. It has been seen that, the volume fraction of solid also increases with sintering temperature.

5.3.2 Contiguity

Figures 5.14a and 5.14b show the contiguity variation in 80W, 85W and 90W alloys with different Ni to Cu ratio sintered at 1440°C and 1460°C respectively. From the figures, the following features are noticed:

1. Decrease in contiguity with increase in the nickel content in binder.
2. Increase in contiguity with increase in the sintering temperature.
3. Increase in contiguity with increase in the tungsten content.

5.3.3 Connectivity

Figures 5.15a and 5.15b show the effect of Ni to Cu ratio on connectivity of 80W, 85W and 90W alloys sintered at 1440°C and 1460°C respectively. It was observed that connectivity decreases with increase in nickel content in binder. It has been also observed that connectivity increases with sintering temperature and tungsten content.

5.3.4 Interface Area of W-W and W-Matrix per Unit Volume

Figures 5.16a and 5.16b depict the effect on binder content on W-W surface area per unit volume of 80W, 85W and 90W alloys sintered at 1440°C and 1460°C respectively.

Figures 5.17a and 5.17b depict the effect on binder content on W-Matrix surface area per unit volume of 80W, 85W and 90W alloys sintered at 1440°C and 1460°C respectively. It was observed that tungsten-matrix surface area increases with decreasing tungsten content in the system.

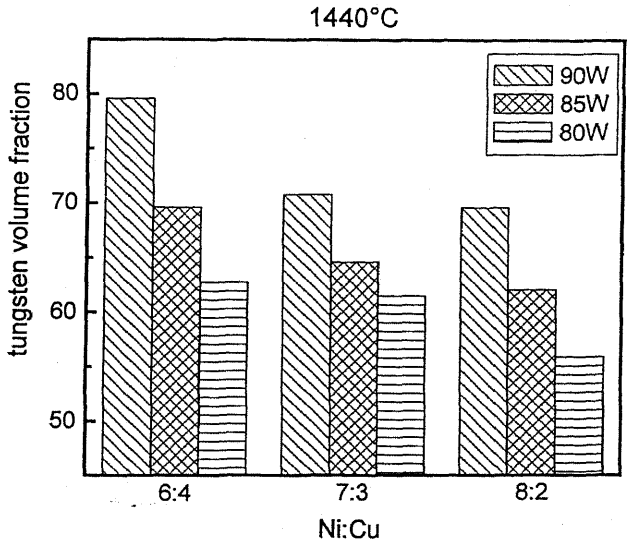

(a)

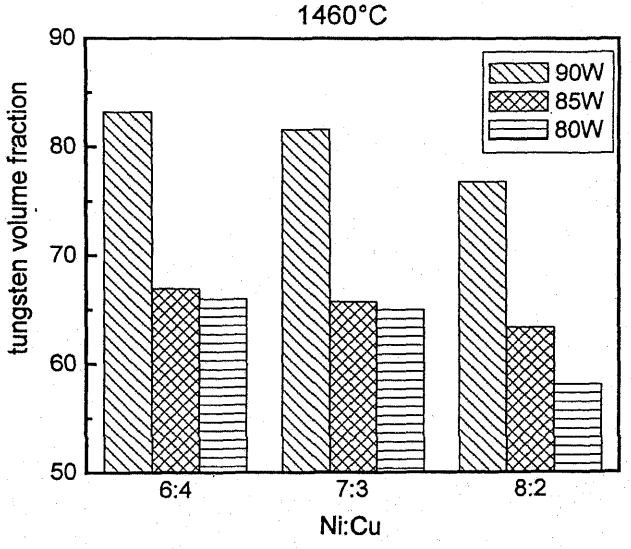

(b)

Figure 5.13. Effect of nickel to copper ratio on tungsten volume fraction of W-Ni-Cu alloys sintered at (a) 1440°C and (b) 1460°C.

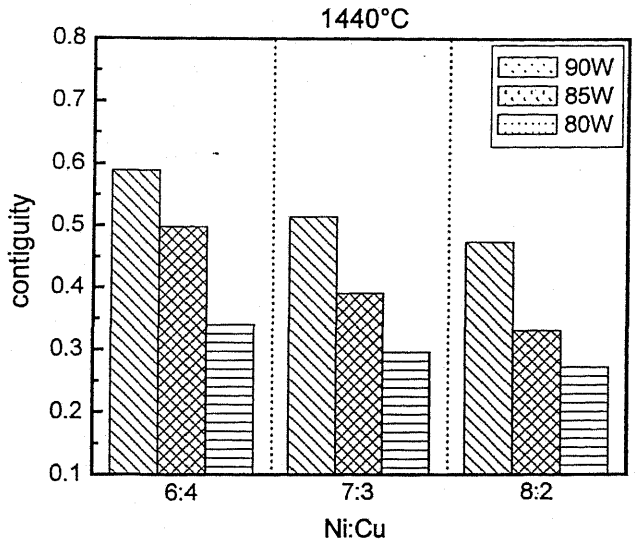

(a)

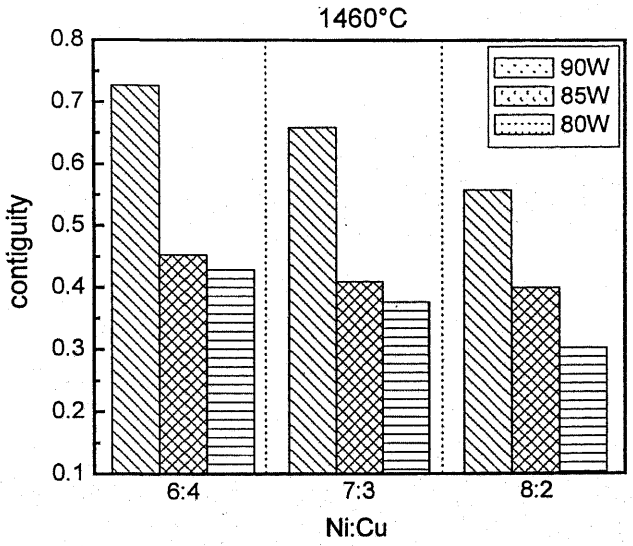

(b)

Figure 5.14. Effect of nickel to copper ratio on contiguity of W-Ni-Cu alloys sintered at (a) 1440°C and (b) 1460°C.

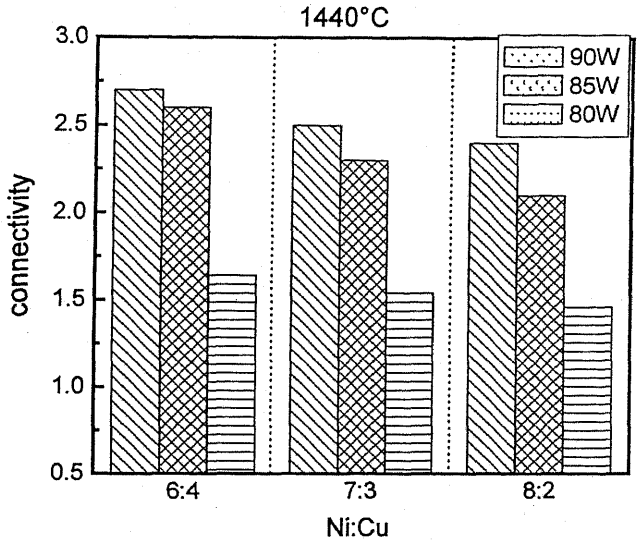

(a)

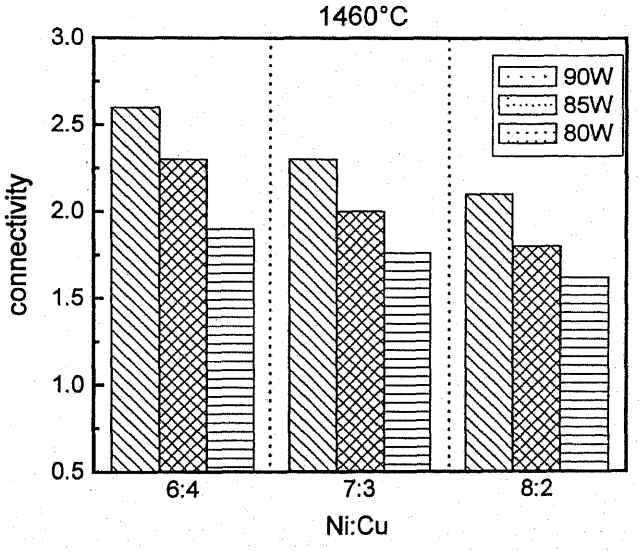

(b)

Figure 5.15. Effect of nickel to copper ratio on connectivity of W-Ni-Cu alloys sintered at (a) 1440°C and (b) 1460°C.

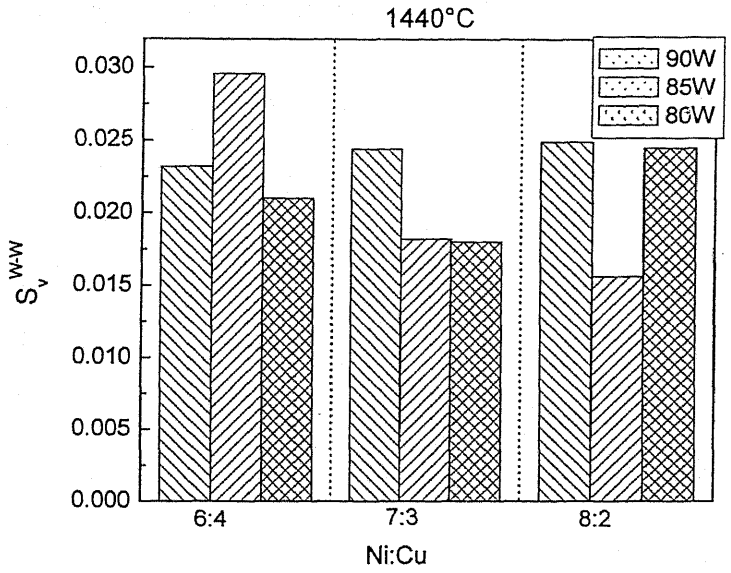

(a)

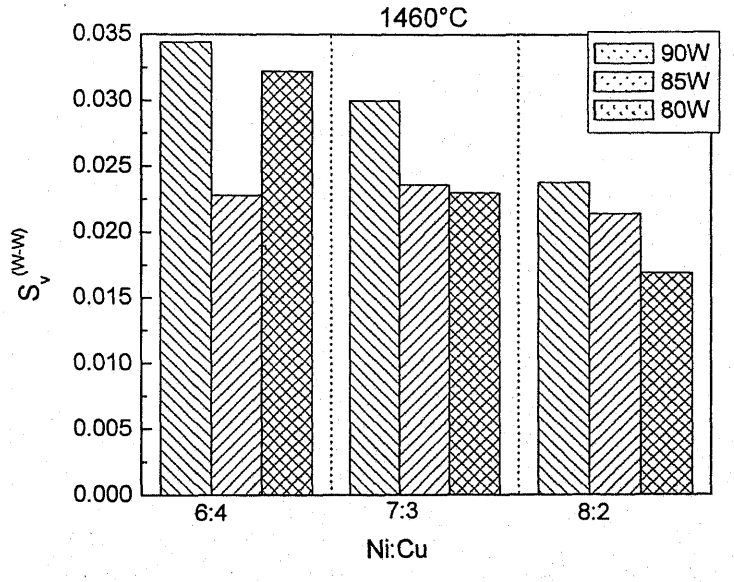

(b)

Figure 5.16. Effect of nickel to copper ratio on W-W interface area per unit volume of W-Ni-Cu alloys sintered at (a) 1440°C and (b) 1460°C.

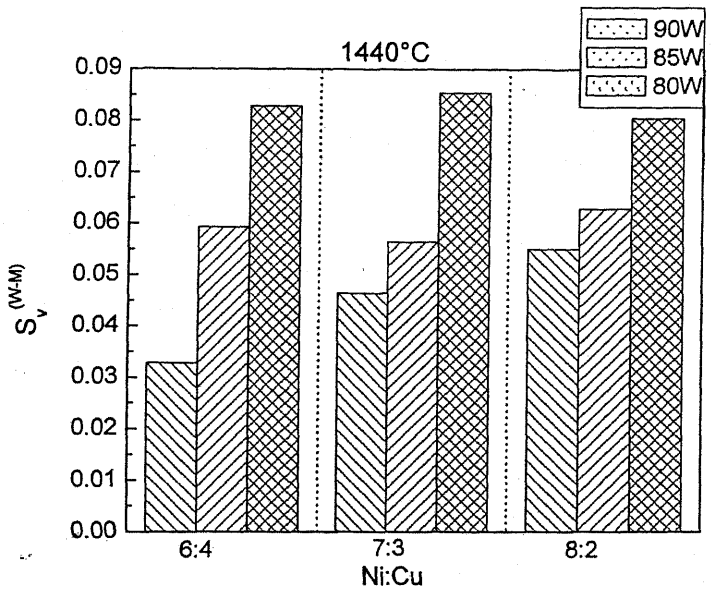

(a)

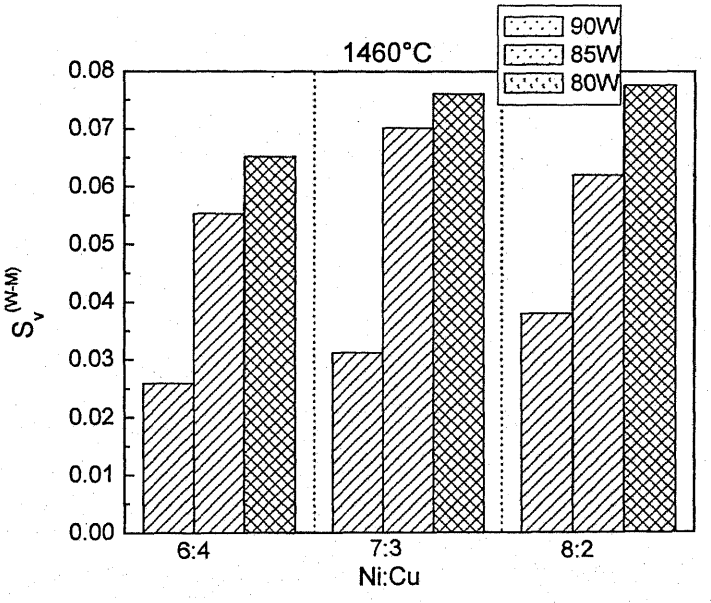

(b)

Figure 5.17. Effect of nickel to copper ratio on W-Matrix interface area per unit volume of W-Ni-Cu alloys sintered at (a) 1440°C and (b) 1460°C.

5.3.5 Mean Grain Size

Figures 5.18a and 5.18b show the average grin size variation in 80W, 85W and 90W alloys with different Ni to Cu ratio sintered at 1440°C and 1460°C respectively. It has seen that average grain size of tungsten increases with copper content in the system. High tungsten content results in higher grain size. It also increases with sintering temperature.

5.3.6 Dihedral Angle (Manual Measurement)

Figure 5.19a and 5.19b show the effect of Ni to Cu ratio on dihedral angle of 80W alloys sintered at 1440°C and 1460°C respectively. They depict that dihedral angle decreases with increase in nickel content up to 7:3. Then again it increases.

Figure 5.20a shows the effect of Ni to Cu ratio on dihedral angle of 85W alloys sintered at 1440°C. As the Ni content increases the dihedral angle decreases. Figure 5.20b shows the dihedral angle variation of 85W alloys with different Ni to Cu ratio sintered at 1460°C. The trend, which is depicted by Figure 5.20a, is more prominent in this case.

Figure 5.21a shows the dihedral angle variation of 90W alloys with different Ni to Cu ratio sintered at 1440°C. This does not follow the same trend as we have seen in case of 85W. Here the dihedral angle first decreases with increase in Ni contents up to 7:3, which is obvious. Subsequently the dihedral increases at the ratio of 8:2. Figure 5.21b shows the dihedral angle variation of 90W alloys with different Ni to Cu ratio sintered at 1460°C. The dihedral angle increases with increase in tungsten content. It follows the same trend as we have seen in Figures 5.20a and 5.20b.

These angles are measured manually on two-dimensional microstructure. There are 200 data points on each sample. The corresponding mean value has been reported.

5.3.7 Dihedral Angle (Automated Measurement)

Automated measurement of dihedral angle is a unique process. Figures 5.22a and 5.22b show the comparison made between the automated measurements and the manual measurements done on the 85W-12Ni-3Cu and 90W-7Ni-3Cu samples

sintered at 1460°C and 1500°C respectively. The two curves match very closely, proving the efficacy of the scheme.

5.4 Mechanical Properties

5.4.1 Macro-Hardness

Figure 5.23 shows the variation in bulk hardness values (VHN) of solid-state sintered compacts sintered at 1360°C. It was observed that hardness values decreased with tungsten content. It was also found that hardness values are less than liquid phase sintered compacts.

Figures 5.24a and 5.24b show the variation in bulk hardness values in 80W, 85W and 90W alloys with different Ni to Cu ratio sintered at 1440°C and 1460°C respectively. It has been found that hardness values are increasing with tungsten content in the system. Hardness value also decreases with increasing nickel content.

5.4.2 Micro-Hardness

Figure 5.25a shows the effect of nickel to copper ratio on micro-hardness of matrix phase of W-Ni-Cu alloys sintered at 1440°C. It has been observed that as the nickel content increases the hardness values increases. The matrix of 80W alloys show higher hardness values compared to other. Figure 5.25b shows the effect of nickel to copper ratio on micro-hardness of tungsten particle of W-Ni-Cu alloys sintered at 1440°C. There is no such significant change in hardness values with respect to sintering temperature.

Figure 5.26a shows the effect of nickel to copper ratio on micro-hardness of matrix phase of W-Ni-Cu alloys sintered at 1460°C. It shows the same trend as we have seen in case of Figure 5.25a.

Figure 5.26b shows the effect of nickel to copper ratio on micro-hardness of tungsten particle of W-Ni-Cu alloys sintered at 1460°C.

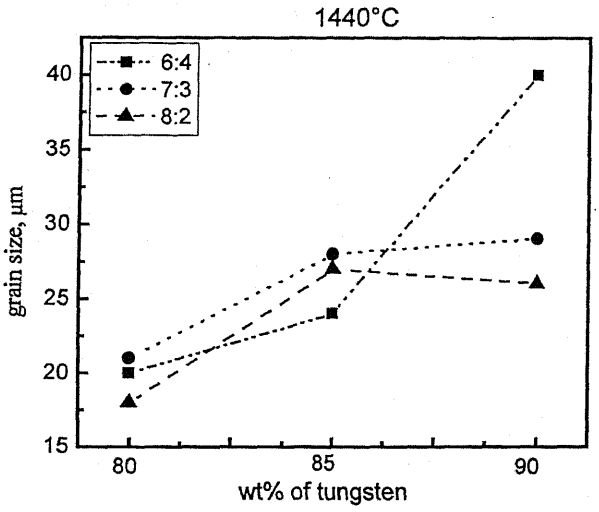

(a)

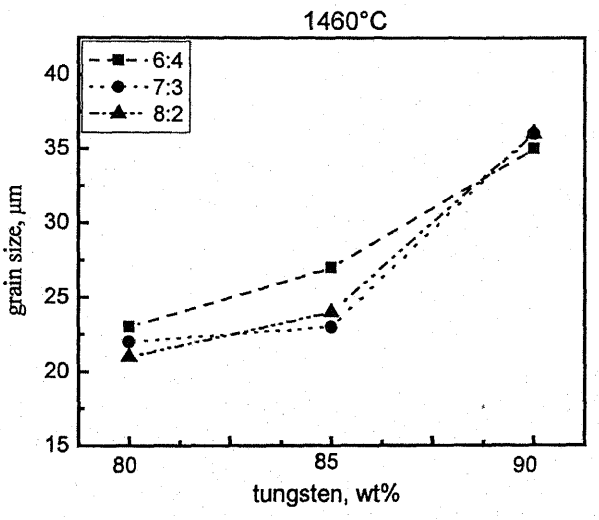

(b)

Figure 5.18. Effect of nickel to copper ratio on average grain size of W-Ni-Cu alloys sintered at (a) 1440°C and (b) 1460°C

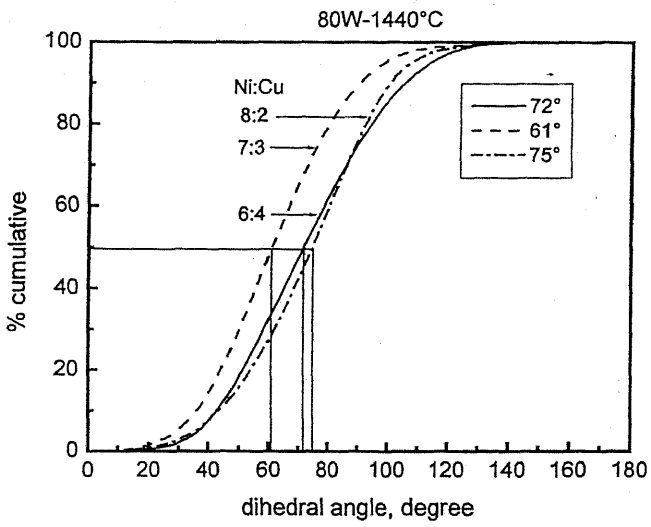

(a)

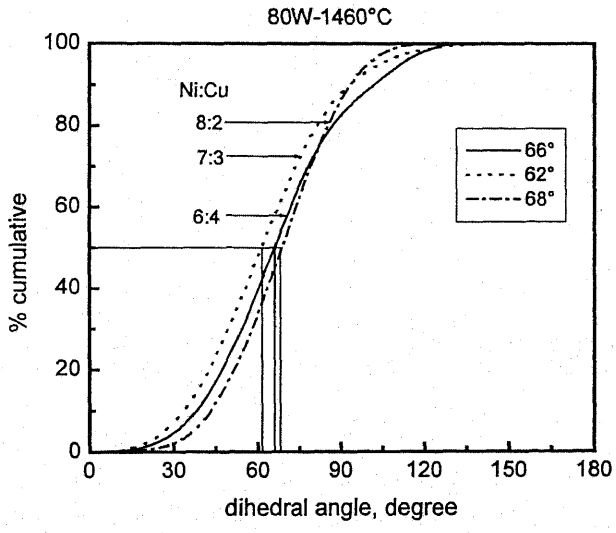

(b)

Figure 5.19. Effect of nickel to copper ratio on dihedral angle of W-20 (Ni-Cu) alloys sintered at (a) 1440°C and (b) 1460°C

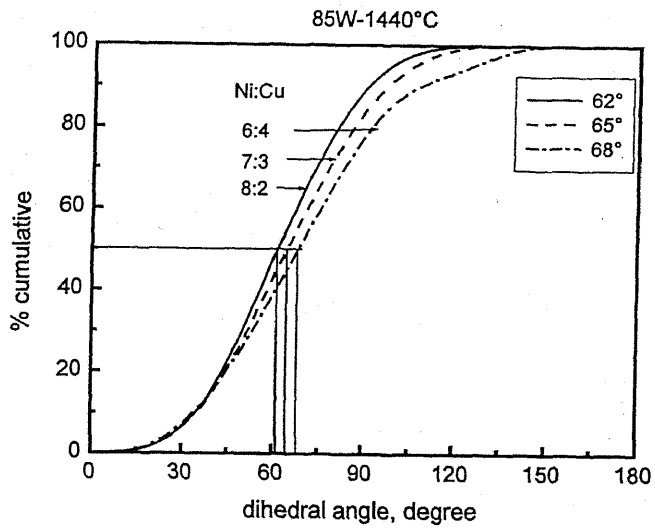

(a)

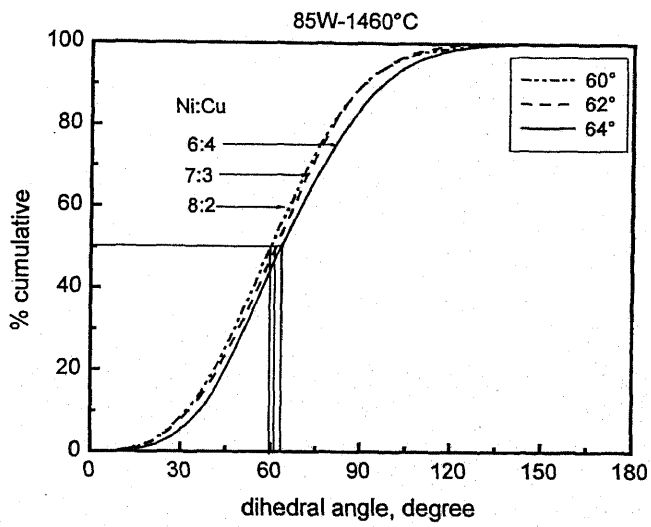

(b)

Figure 5.20. Effect of nickel to copper ratio on dihedral angle of W-15 (Ni-Cu) alloys sintered at (a) 1440°C and (b) 1460°C.

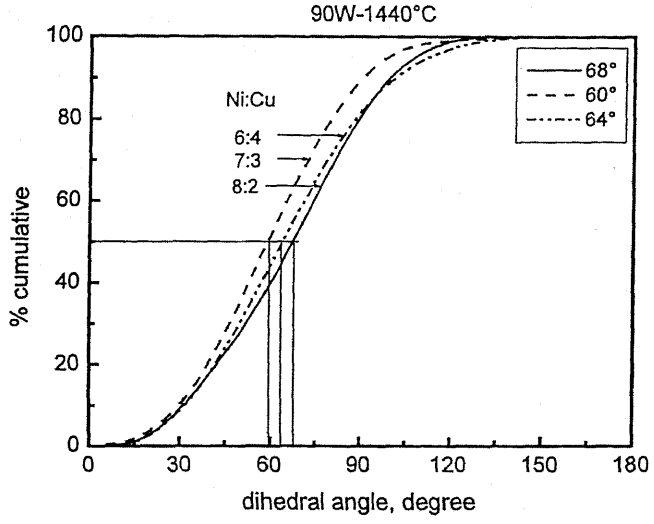

(a)

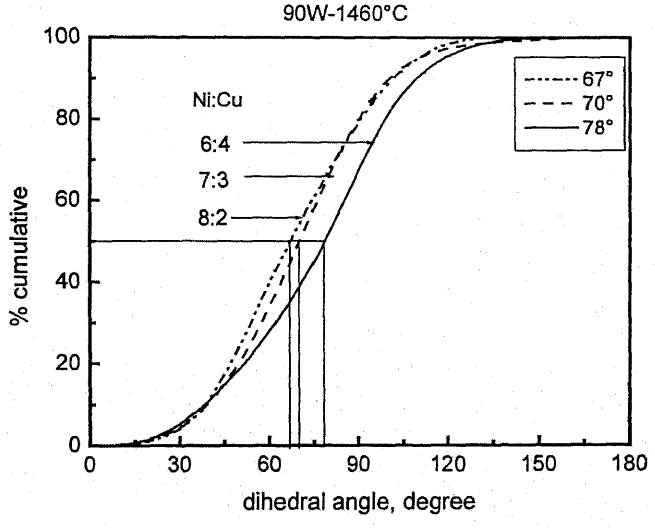

(b)

Figure 5.21. Effect of nickel to copper ratio on dihedral angle of W-10 (Ni-Cu) alloys sintered at (a) 1440°C and (b) 1460°C.

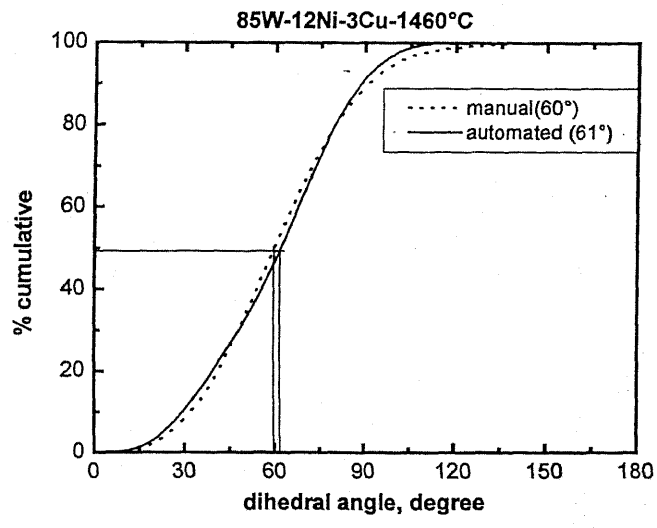

(a)

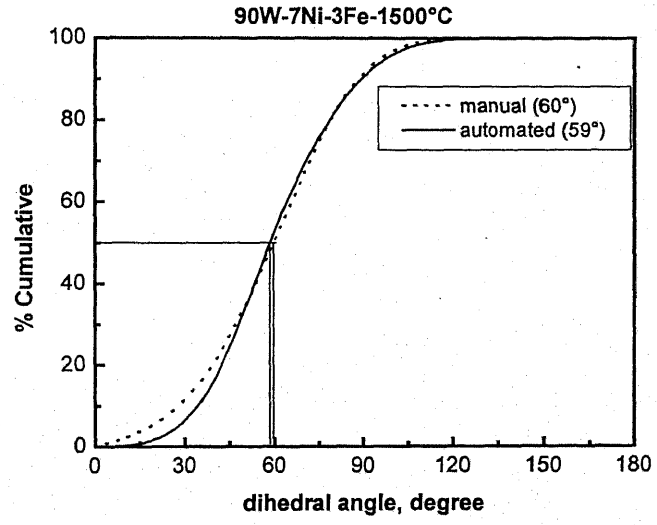

(b)

Figure 5.22. The comparison made between the automated measurements and the manual measurements done on the (a) 85W-12Ni-3Cu (b) 90W-7Ni-3Fe samples sintered at 1460^0 C. and 1500°C respectively.

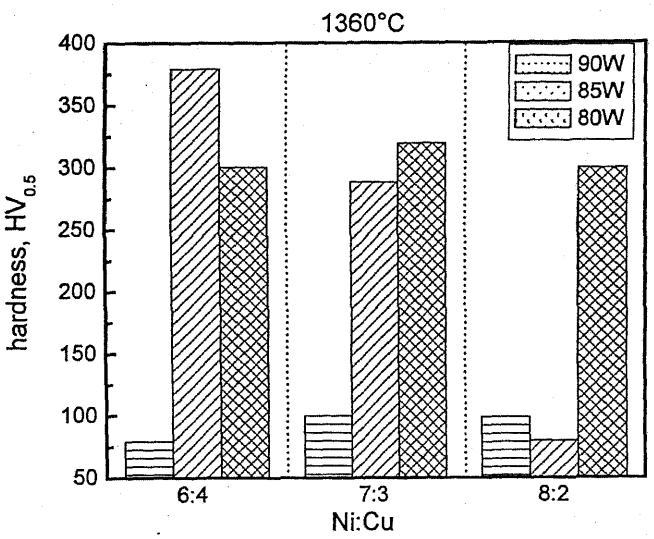

Figure 5.23. Effect of nickel to copper ratio on macro-hardness of W-Ni-Cu alloys sintered at 1360°C.

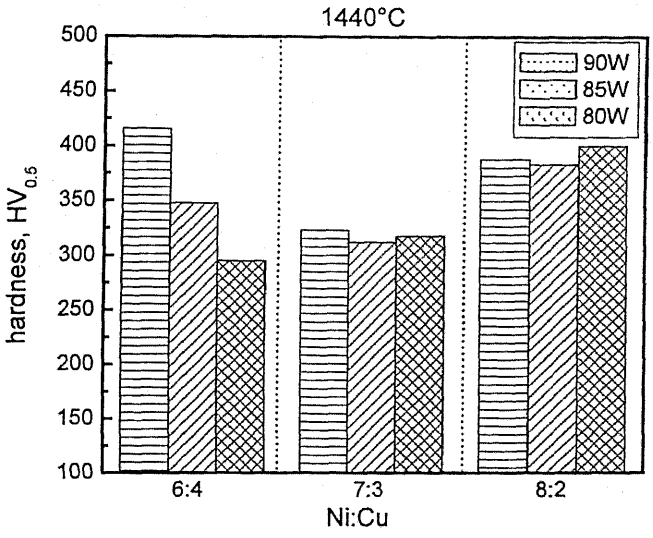

(a)

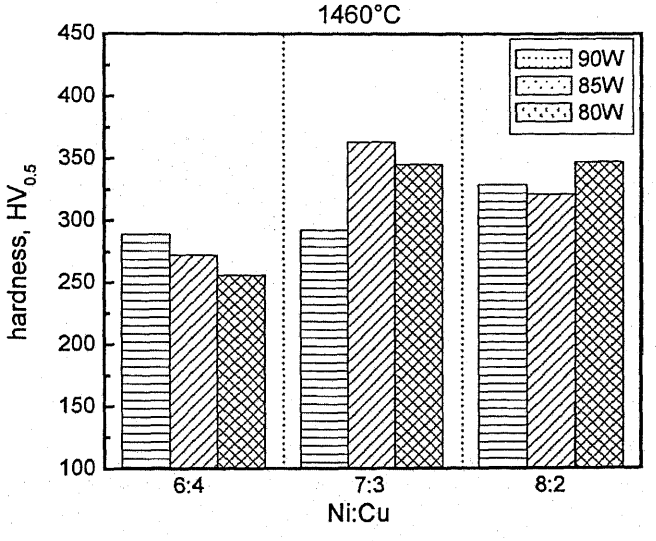

(b)

Figure 5.24. Effect of nickel to copper ratio on macro-hardness of W-Ni-Cu alloys sintered at (a) 1440°C and (b) 1460°C

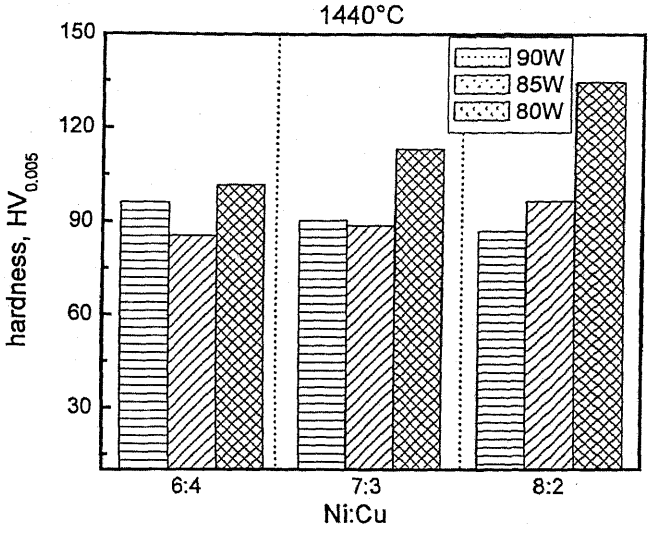

(a)

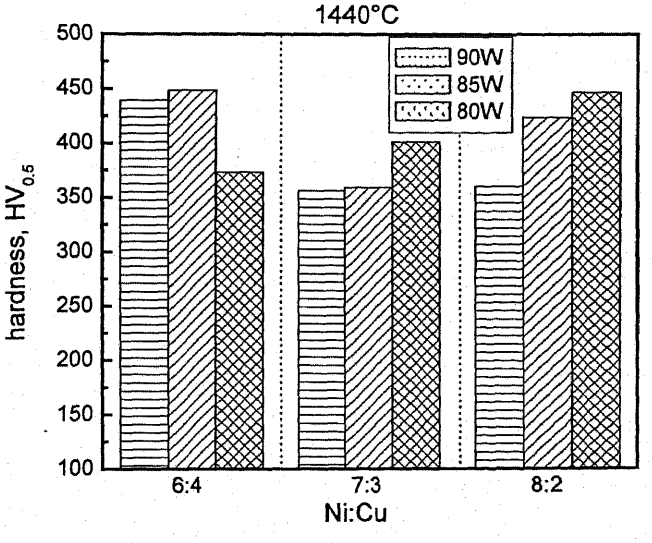

(b)

Figure 5.25. Effect of nickel to copper ratio on micro-hardness of (a) matrix and (b) tungsten of W-Ni-Cu alloys sintered at 1440°C

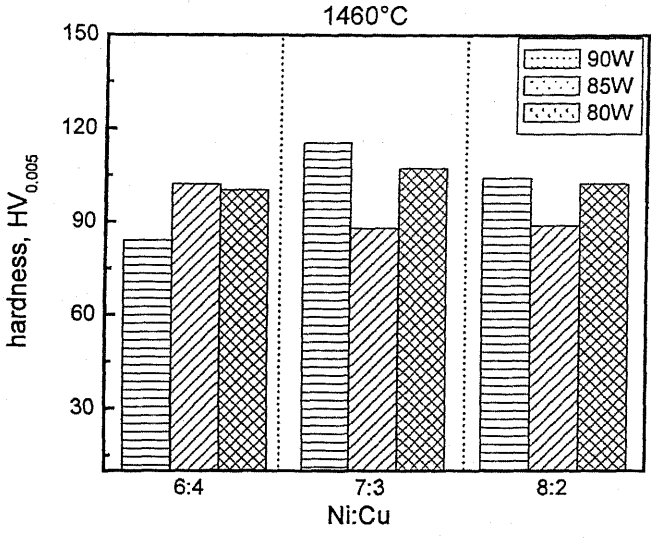

(a)

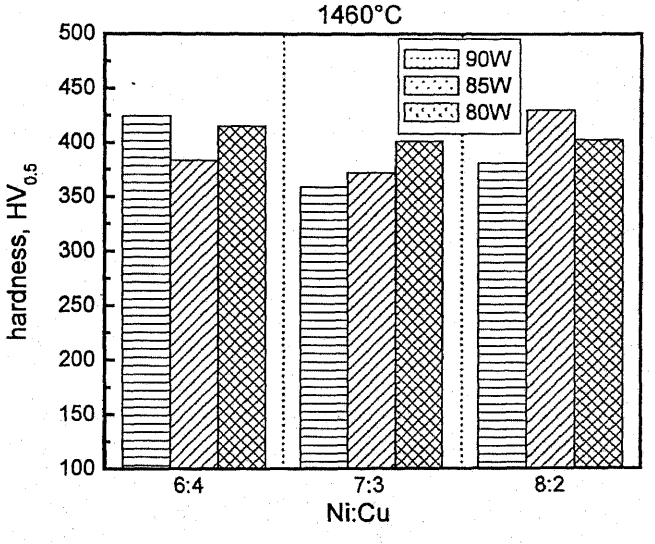

(b)

Figure 5.26. Effect of nickel to copper ratio on micro-hardness of (a) matrix and (b) tungsten of W-Ni-Cu alloys sintered at 1440°C

Chapter 6
DISCUSSION

In this chapter, the results obtained in the present investigation are discussed. In the first section we will summarize the changes in densification behavior of W-Ni-Cu compacts as a function of sintering temperature and binder content of the system. Microstructural features observed in optical microscopy are discussed in next section. Quantitative metallography has been discussed in subsequent sections.

6.1 Densification Behavior

Grain boundary diffusion is mainly responsible for solid-state densification. As the W-W contact area increases, the diffusivity increases which results increasing rate of sintering and higher densification can be achieved.

Liquid phase sintering is the predominated mechanism to produce near full density heavy alloys. The classic liquid phase sintering system consists of three overlapping stages as shown in the figure 2.4. Rearrangement or liquid flow is the first stage. It corresponds to large-scale bulk movement of particles with in liquid phase. This movement leads to rearrangement of particles and densification. Capillary force exerted by the wetting liquid on the solid particles is responsible for the bulk movement of the particles in the liquid phase. The elimination of porosity occurs as the system minimizes its surface energy. The compact responds as a viscous solid to the capillary action during rearrangement stage. As a consequence, the densification attainted in rearrangement stage is dependent on the amount of liquid, particle size, and solubility of solid in the liquid. It is estimated that 35 vol.% of liquid is needed to obtain full density by rearrangement process. Usually finer particles give better rearrangement.

Solution-reprecipitation is the next stage of liquid phase sintering. It is characterized by solution and diffusivity effects. This stage is related with microstructural coarsening and it is due to distribution in grain sizes. Grain size plays an important role in grain dissolution. The solubility of a grain in a liquid varies inversely with grain size. That implies small grains have higher solubility than coarse grains. Thus, concentration gradient establishes in liquid due to difference in solubility. Material is transported from

the small grains to the larger grains by diffusion. This process is called as Oswald ripening or coarsening. The net result is a progressive growth of the larger grains, giving a fewer grains with wider spacing. This stage is not only responsible for grain coarsening but also to densification. This process leads to pore elimination as well as grain shape accommodation.

The last stage of this classical sintering is referred to as solid-state sintering. Densification is slow in this case because of the existence of solid skeleton. The rigidity of the solid skeleton inhibits further rearrangement but microstructural coarsening continues by diffusion. This stage leads to poor sintered properties. Hence, short sintering periods are preferred in practice.

At the sintering temperature of 1440°C and 1460°C, the binary binder composition of Ni:Cu is in the liquid state. Thus, the liquid phase sintering mechanism is therefore applicable through particle rearrangement and solution-reprecipitation process. Researchers reported that the dihedral angle between tungsten and Cu-Ni binder is small [29]. The liquid phase penetration along grain boundaries is more prominent, thereby enhancing solution reprecipitation mechanism. The kinetics is faster when the contact surface is more between the tungsten and matrix. That is why the densification is slower for low mass% of the binder for any sintering period.

The reason for increased densification with sintering temperature may be attributed to the efficient spreading of the binder melt at elevated temperature.

6.2 Microstructure Evolution

It seems that liquid phase sintering is incomplete in alloys with Ni to Cu ratio 8:2. It may be because of low homologous temperature. The samples were sintered at three different homologous temperatures. The solidus temperatures of alloy containing nickel and copper in the ratio 6:4, 7:3, and 8:2 are 1285°C, 1325°C, and1360°C respectively. The driving force for liquid phase sintering is insufficient in case of 8:2 samples. Wetting liquid puts grains into contact. Grain coalescence is a possible intermediate stage densification and coarsening mechanism in tungsten-based heavy alloys. Grains with differing sizes, the driving force for coalescence is boundary migration due to curvature. As the Nickel content increases the amount of grain

coalescence decreases. Tungsten is insoluble in Copper but it has substantial solubility in Nickel. The solubility of tungsten in matrix increases with increase in nickel content. It decreases the amount of grain coalescence, which is seen in the microstructure containing Ni to Cu ratio 7:3 and 8:2. Because of insufficient temperature difference from the solidus temperature in Ni-Cu isomorphous system the microstructure containing higher nickel to copper ratio (8:2) does not show the same trend. The driving force for liquid phase sintering is insufficient in case of 8:2 samples.

Grain growth takes place at higher sintering temperature. Due to high sintering temperature as compared to 1440°C and high W content, grain coalescence is the basic feature of these microstructures. Increase in Ni content decreases the grain coalescence in the sintered specimen. This is because of higher solubility of tungsten into the matrix.

6.3 Quantitative Metallography

6.3.1 Volume Fraction of Solid

There are initially three phases – solid, liquid and pore for a liquid phase sintered system. Generally, the objective during liquid phase sintering is to eliminate the pores. For persistent liquid phase sintering, the volume fraction of solid and liquid become constant at long sintering times. Matrix phase, in tungsten heavy alloys, is mainly a solid solution of tungsten in binding elements (Ni, Cu, Fe). Formation of intermetallics may possible depending upon the interaction of binders with tungsten. Maximum solubility of tungsten in the binder metal falls in the sequence Ni (40%)-Co (35%)-Fe (33%). Volume fraction decreases with increasing amount of nickel in the system. This is because of solubility effect. Tungsten has no solubility in Copper but it is soluble in nickel. In the binder phase the solubility of tungsten increases as the amount of nickel increases in the binder phase. Therefore, the dissolution of tungsten in binder is more in high nickel to copper ratio. Thus, the volume fraction of solid is less in higher nickel to copper ratio. The grain coalescence is more prominent in system having higher amount of copper. It is one of the reasons of higher volume fraction of solid. At higher sintering temperature the grain growth takes place. This is the reason of higher value of solid volume fraction at higher temperature. The microstructural changes associated with an increasing volume

fraction of solid are quite pronounced. More solid-solid contacts form at the higher volume fraction of solid.

6.3.2 Contiguity

The contiguity is a measure of the solid-solid contact in a liquid phase sintered material. The dihedral angle and volume fraction of solid have a large effect on the contiguity. Change in the dihedral angle provides substantial change in the contiguity. For a fixed W content, contiguity decreases with increase in nickel content. This is because of the higher solubility of W in matrix with higher amount of Ni content. As a result of which the amount of W-W contact area decreases, thereby reducing the contiguity of the microstructure. On the other hand as the temperature increases the contiguity for a fixed composition increases because of grain growth.

6.3.3 Connectivity

The number of contacts per solid grain determines the microstructural connectivity. The solid-solid contacts are stabilized by a non-zero dihedral angle. As a consequence the solid structure forms a rigid skeleton. Contacts per grain increases with the volume fraction of solid. It follows the same trend as shown by contiguity. Microstructural coarsening does not have a significant effect on the connectivity.

6.3.4 Interface Area of W-W and W-Matrix per Unit Volume

In previous chapter it has seen that tungsten-matrix interface area increases with decreasing tungsten content in the system. It is because of increasing contiguity in the system. As the tungsten content increases the W-W contact area increases which in turn reduces the W-Matrix interface area in the system. Solubility of tungsten particle in the matrix phase increases with nickel content in the system. Thus, the W-W contact area in the system reduces. There is little change in W-matrix area with temperature. As the temperature increases the W-W area increases because of grain growth. A coalescence phenomenon is an intermediate stage of densification of tungsten heavy alloys. Grain growth occurs at elevated temperature by coalescence. Thus, it is responsible for lower

value of W-matrix contact area. Compacts with higher amount of binder will have high W-matrix contact area.

6.3.5 Grain Size

Grain growth takes place at higher sintering temperature. The average grain size increases because of grain growth. It also depends upon the amount of tungsten content in the system. The effect of sintering temperature on grain size is more prominent at higher tungsten content. Solubility effect has a significant role on average grain size. Grain coalescence leads to higher average grain size. High amount of copper content in the system is responsible for grain coalescence. The high average value of grain size leads to high dihedral angle.

6.3.6 Dihedral Angle (Manual Measurement)

The dihedral angle is formed where a solid-solid grain boundary intersects the liquid. The dihedral angle is important to the microstructure of polycrystalline grains and to grain-grain contacts in the liquid phase. This angle is characteristic of the energy ratio between the grain boundaries and solid-liquid surfaces.

A change in the energy of either the solid-solid grain boundary or the solid-liquid surface results in a change in the dihedral angle. Dihedral angle decreases with increase in nickel content up to 7:3. From the microstructure point of view, we may conclude that grain coalescence causes the increase in dihedral angle. Grain coalescence leads to more W-W contact, which means more contact area. Interfacial energy between solid-solid increases due to increase in contact area. This means decrease in dihedral angle. The solubility of tungsten particle into nickel-copper matrix increases as the amount of nickel increases in the system. This, in turn, reduces the tungsten- tungsten contact area, which results decrease in dihedral angle. As the temperature increases the average grain size also increases, which leads to decrease in dihedral angle with higher amount of Ni content.

90W alloys show different trend. Here the dihedral angle first decreases with increase in Ni contents up to 7:3, then again it increases at the ratio of 8:2. This may be due to incomplete liquid phase sintering.

The dihedral angle increases with increase in tungsten content, which leads to more W-W contact area. Because of higher average grain size at higher temperatures the dihedral angle also increases for a fixed composition.

6.3.7 Dihedral Angle (Automated Measurement)

The scheme of image processing and analysis developed was applied to Tungsten-Nickel-Copper alloys for the determination of the distribution of dihedral angles.

In order to ensure measurement accuracy of dihedral angles by the automated technique, the correlation coefficients of the best-fit polynomials were checked. A statistical sample of manual measurements was compared with automated measurements along with the correlation coefficients. By such comparisons it was observed that in the case of each large discrepancy between manual and automated measurement the correlation coefficient for one or more of the best-fit polynomial was less than 0.60 [44]. Thus for all subsequent automated measurements of plane dihedral angles, if the correlation coefficient was less than 0.60 then the associated neck point was rejected from the analysis.

6.4 Mechanical Properties

6.4.1 Macro-Hardness

Hardness depends upon the microstructure. For the typical case of a harder solid grain dispersed in the solidified matrix, the matrix has the greater ductility. The hard phase provides strengthening to the matrix and decreases the dislocation motion during deformation. However, the matrix properties control the overall hardness. As a consequence the composite hardness depends on the volume fraction of the harder phase. The hardness decreases as the amount of matrix increases. Also, the hardness decreases as the grain size increases, due to a greater separation of grains. A high contiguity aids the hardness because of greater rigidity from the solid-solid contacts. As the tungsten content increases the volume fraction of harder phase also increases. This provides more

contiguous structure, which leads higher hardness value. As the nickel content in the binder increases the dissolution of solid tungsten into the matrix increases, which in turn lowers the volume fraction of tungsten. The solid-state sintered compacts show less hardness than liquid phase sintered compacts. This is because of less densification of compacts at 1360°C.

6.4.2 Micro-Hardness

In tungsten heavy alloys, tungsten is harder phase and softer phase is matrix. The matrix forms by nickel and copper having some dissolved tungsten. Tungsten has solubility in nickel but it hardly dissolves into copper. Thus, as the nickel content in the binder increases the amount of dissolved tungsten in the matrix increases. The dissolved tungsten provides more hardness in matrix. Therefore, it has been observed that the hardness of matrix phase increases with increasing nickel to copper ratio. It was also found that as the volume fraction of matrix increases higher amount of tungsten gets dissolved into matrix, which in turn increases hardness of matrix phase.

Chapter 7
CONCLUSIONS

Considering results and discussions of the present investigation, the following conclusions can be drawn:

1. Liquid phase sintering is the predominant mechanism of densification of W-Ni-Cu alloys. It provides better-sintered density than solid-state sintering.
2. In case of W-Ni-Cu system the interrelated parameters of contiguity and connectivity decreases with increase in nickel content in the system. As the nickel content increases in the binder, the dissolution of tungsten particles increases in the matrix phase. Thus, contiguity and connectivity decreases.
3. Volume fraction of solid increases with tungsten content and decreases with nickel content in the system.
4. Interfacial area of tungsten-matrix increases with nickel content in the system and it decreases with amount of tungsten.
5. There is no such influence of temperature on tungsten-matrix interfacial area in this study.
6. In the case of W-Ni-Cu system, the average grain size increases with increase in tungsten content and decreases with increase in nickel content in the system.
7. Grain coarsening occurs at higher sintering temperature.
8. Coalescence is a possible densification and grain coarsening mechanism
9. In the W-Ni-Cu alloys, the dihedral angle increases with increase in tungsten content and decreases with increase in nickel content in the system.
10. There is no such significant change in contiguity, connectivity, grain size, and dihedral angle with increase in sintering temperature.
11. Liquid phase sintering provides homogeneous microstructure in W-Ni-Cu system.
12. A new and unique methodology has been developed to measure dihedral angle of liquid phase sintered tungsten heavy alloys automatically from two-dimensional microstructure. Dihedral angles of these samples, measured manually and automatically, were compared and the results so obtained corroborated the efficacy of the scheme developed for evaluating dihedral angles.

13. Bulk hardness of compacts increases with tungsten content of the system.
14. Hardness of matrix phase increases with increasing nickel content of the system. There is a little change in hardness value with increasing sintering temperature.

REFERENCES

1 E. Lassner and W.D. Schubert, Tungsten, Kluwer Academic / Plenum Publishers, New York, NY, USA, 1999.

2 A. Upadhyaya, "Processing Strategy for Consolidating Tungsten Heavy Alloys for Ordnance Applications," *Journal of Material Chemistry and Physics,* 2001, v. 67, pp. 101-110.

3 www.mallory.com

4 S.G. Caldwell, "Tungsten Heavy Alloys," ASM Hand Book, P.W. Lee and R. Lacocca (eds.), Materials Park, Ohio, USA, 1998, v. 7, pp. 914 –921.

5 E. Ariel, J. Barta and D. Brandon, "*Powder Metallurgy International*, 1973, v. 5, pp. 125-128.

6 A. Belhadjhamida and R.M. German, "Tungsten and Tungsten Alloys by Powder Metallurgy- A Status Review," Tungsten and Tungsten Alloys-Recent Advances, Andrew Crowson, and Edward S. Chen (eds.), The Minerals, Metals & Materials Society, 1991, pp. 3-19.

7 R.M. German, Powder Metallurgy Science, 2nd Edition, Metal Powder Industries Federation, Princeton, NJ, USA, 1994.

8 C.J. Smithells, 'Tungsten, its Metallurgy, Properties and Applications', Chemical publishing Co. Inc. New York, 1953, pp. 258.

9 G.S. Upadhyaya, Powder Metallurgy Technology, Cambridge International Science Publishing, Cambridge, England, 1997.

10 R.M. German, Sintering Theory and Practice, John Wiley, New York, NY, USA, 1996.

11 J.H. Brophy and A.L. Prill, "A Reanalysis of Data on the Solution-Reprecipitation Stage of Liquid Phase Sintering," *Transaction AIME*, vol. 236, 1966, pp. 85-91.

12 A.L. Prill *et al.*, "The Role of Phase Relationships in the Activated Sintering of Tungsten," *Transaction AIME*, vol. 230, 1964, pp. 769-772.

13 F.V. Lenel, "Fundamentals in Sintering," *Transaction AIME*, vol. 175, pp. 878-881, 1948.

14 R.M. German, Liquid Phase Sintering, Plenum Press, New York, USA, 1985.

15 W.D. Kingery, "Densification during Sintering in The Presence of a Liquid Phase 1. Theory," *Journal of Applied Physics*, 1959, v. 30, pp. 301-306.

16 J.S. Lee, H.H. Hwang, and H. Shin, "Influence of Ni-P Alloy Addition in the Formation of W-Skeleton," *International Journal of Refractory and Hard Metals*, 1990, v. 9, pp. 46-49.

17 V. Smolej, S. Pejovnic, and W.A. Kaysser, "Rearrangement during Liquid Phase Sintering of Large Particles," *Powder Metallurgy International*, 1982, v. 14, pp. 34-36.

18 W.J. Huppmann and H. Riegger, "Liquid Phase Sintering of the Model System W-Ni," *International Journal of Powder Technology*, 1977, v. 13, pp. 242-247.

19 R.M. German and J.L Johnson, "Chemically Activated Liquid Phase Sintering of W-Cu," *International Journal of Powder Metallurgy*, 1994, v. 30, n. 1, pp. 91-102.

20 W.A. Kaysser, O.J. Kwon, and G. Petzow, "Pore Formation and Pore Elimination during Liquid Phase Sintering," Proceedings of International Powder Metallurgy Conference, Associazione Italiana di Metallurgia, Florence, Italy, 1982, v. 6, pp. 23-30.

21 S. Farooq, A. Bose, and R.M. German, "Theory of Liquid Phase Sintering: Modern Experiments on W-Ni-Fe Heavy Alloy System," Progresses in Powder Metallurgy, Metal Powder Industries Federation, Princeton, NJ, USA, 1987, v. 43, pp. 65-77.

22 R.M. German and S. Farooq, "An Update on the Theory of Liquid Phase Sintering," Sintering 87, Applied Science Pub., London, UK, 1988, v. 1, pp. 459-464.

23 W.A. Kaysser, M. Zivcovic, and G. Petzow, "Shape Accommodation during Grain Growth in the Presence of a Liquid Phase," *Journal of Material Science*, 1985, v. 20, pp. 578-584.

24 S.K. Rout, "Effect of Thermo-Mechanical Treatment on Stereological Aspects of W-Ni-Fe Alloys," M.Tech. Thesis, IIT Kanpur, India, 2002.

25 L.L. Bourguignon and R.M. German, "Sintering Temperature Effects on a Tungsten Heavy Alloy," *International Journal of Powder Metallurgy*, 1988, v. 24, No. 2, pp. 115-121.

26 R.M. German, A. Bose and S.S. Mani, "Sintering time and Atmosphere influences on the Microstructure and Mechanical Properties of Tungsten Heavy Alloy," *Metallurgical Transaction A*, 1992, v. 23, pp. 211-219.

27 K.S. Churn and R.M. German, "Fracture Behavior of W-Ni-Fe Heavy Alloys," *Metallurgical Transactions A*, 1984, v. 15, pp. 747-754.

28 G.H.S. Price, C.J. Smithells, and S.V. Williams, "Sintered alloys. Part I. –Copper-Nickel-Tungsten Alloys Sintered with a Liquid Phase Present," *Journal of Institute. Metals*, vol. 62 (1938) pp. 239.

29 N.C. Kothari, "Densification and Grain Growth during Liquid Phase Sintering of Tungsten-Nickel-Copper alloys," *Journal Less-Common. Metals*, vol. 13, 1967, pp. 457.

30 R. Makarov, O.K. Teodorovich and I.N. Fruntsevich, "The Coalescence Phenomena in Liquid Phase Sintering in the Systems W-Ni-Fe and W-Ni-Cu," *Soviet Powder Metallurgy and Metal ceramic*, vol. 4, 1965, pp. 554-559.

31 V. Srikanth and G.S. Uadhyaya, "Modern Developments Powder Metallurgy," 1985 v. 15-17, MPIF, Princeton, NJ.

32 K.N. Ramakrishnan and G.S. Upadhyaya, "Effect of Composition and Sintering on the densification and microstructure of heavy alloys containing copper and nickel", *Journal of Materials Science Letters*, vol. 9, 1990, pp. 456-459.

33 J.F. Kuzmic, Modern Development in Powder Metallurgy, Ed. H.H. Hausner, 1966, v. 3, pp. 166, Plenum Press New York.

34 S. Takajo, W.A. Kaysser, and G. Petzow, "Particle growth by Coalescence during Liquid Phase Sintering of Fe-Cu," *Acta Metallurgica,* 1984, v. 32, pp 107-113.

35 C.M. Kipphut, A. Bose, S. Farooq, and R.M. German, "Gravity and Configurational Energy Induced Microstructural Changes in Liquid Phase Sintering," *Metallurgical Transaction A*, 1988, v. 19A, pp. 1905-1913.

36 S.S. Mani and R.M. German, "Kinetics and Gravity Induced Distortion in Liquid Phase Sintering," Advances in Powder Metallurgy-1990, v. 1, Metal Powder Industries Federation, Princeton, NJ, 1990, pp. 453-467.

37 A. Upadhyaya, "A Microstructure-Based Model for Shape Distortion During Liquid Phase Sintering," Ph.D.Thesis, Penn State, USA, 1998.

38 R.M. German, "The Contiguity of Liquid Phase Sintered Microstructures," *Metallurgical Transactions A*, 1985, v. 16A, pp. 1247-1252.

39 V. Srikanth and G.S. Upadhyaya, "Contiguity Variation in Tungsten Spheroids of Sintered Heavy Alloys," *Metallography*, 1986, v. 19, pp. 437-445.

40 J. Gurland, "An estimate of contact and contiguity of dispersions in opaque samples," *Transactions TMS-AIME*, 1966, vol. 236, pp. 642-646.

41 O.K. Riegger and L.H. Van Vlack, "Dihedral Angle Measurement", *Transactions TMS-AIME*, 1960, vol. 218, pp. 933-935.

42 S. Sangal, "Application of Stereology for the Estimation of Dihedral Angle Distribution in Polycrystals", *Metals, Materials & Processes*, 1998, vol. 10, No. 4, pp. 313-322.

43 S. Chhabra, P. Chhillar, and S. Sangal, "Characterization of triple Junction Geometry in Polycrystals by Automated Digital Image Processing," Practical Metallography, 2003, v. 40, no. 2, pp. 85-97.

44 P. Chhillar, "Automated Dihedral Angle Measurement in Liquid Phase Sintered Alloys," B. Tech. Thesis, IIT, Kanpur, India, 2003.

Appendix I

Cylindrical compacts prepared by mixed powders, sintered at 1360°C, 1h, H_2 atmosphere (Compaction Pressure – 200MPa)

Parameters		Alloys		
		80W-12Ni-8Cu	80W-14Ni-6Cu	80W-16Ni-4Cu
Height (cm.)	Green	1.00	1.18	0.85
	Sintered	0.762	1.058	0.784
Diameter (cm.)	Green	0.81	0.81	0.81
	Sintered	0.714	0.714	0.71
Weight (g)	Green	5.1884	6.1661	4.3542
	Sintered	4.3652	5.96	4.1919
Density (g/cm^3)	Green	10.07381	10.14586	9.94603
	Sintered	14.31473	14.07649	13.51165
% Theo. Density	Green	64.35295	64.82149	63.55291
	Sintered	91.44454	89.93416	86.33644
Densification Parameter		0.759995	0.713864	0.625113

Cylindrical compacts prepared by mixed powders, sintered at 1360°C, 1h, H_2 atmosphere (Compaction Pressure – 200MPa)

Parameters		Alloys		
		85W-9Ni-6Cu	85W-10.5Ni-4.5Cu	85W-12Ni-3Cu
Height (cm.)	Green	0.62	0.796	0.700
	Sintered	0.55	0.71	0.594
Diameter (cm.)	Green	0.81	0.81	0.81
	Sintered	0.712	0.72	0.714
Weight (g)	Green	3.3605	4.2122	3.7361
	Sintered	3.3521	4.2094	3.4323
Density (g/cm^3)	Green	10.5238	10.27439	10.36289
	Sintered	15.31527	14.56891	14.43885
% Theo. Density	Green	64.05233	62.54197	63.08448
	Sintered	93.21527	88.68343	87.89708
Densification Parameter		0.811261	0.697887	0.672146

Parameters		Alloys		
		90W-6Ni-4Cu	90W-7Ni-3Cu	90W-8Ni-2Cu
Height (cm.)	Green	0.714	0.786	0.59
	Sintered	0.674	0.778	0.579
Diameter (cm.)	Green	0.81	0.81	0.81
	Sintered	0.71	0.708	0.714
Weight (g)	Green	4.0025	4.4059	3.3131
	Sintered	3.922	4.394	3.302
Density (g/cm^3)	Green	10.88412	10.8836	10.90292
	Sintered	14.70488	14.35305	14.25058
% Theo. Density	Green	62.96132	62.96191	63.081
	Sintered	85.0632	83.03282	82.44953
Densification Parameter		0.596724	0.541899	0.524622

Appendix II

Cylindrical compacts prepared by mixed powders, sintered at 1440°C, 1h, H_2 atmosphere (Compaction Pressure – 200MPa)

Parameters		Alloys		
		80W-12Ni-8Cu	80W-14Ni-6Cu	80W-16Ni-4Cu
Height (cm)	Green	0.50	0.51	0.56
Diameter (cm)	Green	1.279	1.28	1.277
Weight (g)	Green	5.896	6.060	6.641
	Sintered	5.88	6.07	6.66
Volume (cm^3)	Green	0.64	0.66	0.72
	Sintered	0.40	0.41	0.47
Density (g/cm^3)	Green	9.18	9.20	9.22
	Sintered	14.81	14.89	14.07
% Theo. Density	Green	58.66	58.80	58.88
	Sintered	94.64	95.12	89.89
Densification Parameter		0.87	0.88	0.75

Cylindrical compacts prepared by mixed powders, sintered at 1440°C, 1h, H_2 atmosphere (Compaction Pressure – 200MPa)

Parameters		Alloys		
		85W-9Ni-6Cu	85W-10.5Ni-4.5Cu	85W-12Ni-3Cu
Height (cm)	Green	0.61	0.43	0.37
Diameter (cm)	Green	0.804	0.804	0.804
Weight (g)	Green	2.893	2.010	1.763
	Sintered	2.88	2.00	1.75
Volume (cm^3)	Green	0.31	0.22	0.19
	Sintered	0.18	0.14	0.13
Density (g/cm^3)	Green	9.35	9.21	9.52
	Sintered	15.73	14.02	13.82
% Theo. Density	Green	56.90	56.09	57.96
	Sintered	95.73	85.33	84.14
Densification Parameter		0.9010	0.6659	0.6226

Parameters		Alloys		
		90W-6Ni-4Cu	90W-7Ni-3Cu	90W-8Ni-2Cu
Height (cm)	Green	0.43	0.42	0.46
Diameter (cm)	Green	0.804	0.804	0.804
Weight (g)	Green	2.102	2.023	2.373
	Sintered	2.10	2.02	2.37
Volume (cm^3)	Green	0.22	0.21	0.23
	Sintered	0.13	0.13	0.14
Density (g/cm^3)	Green	9.68	9.54	10.10
	Sintered	16.39	16.14	16.88
% Theo. Density	Green	56.00	55.19	58.44
	Sintered	94.80	93.39	97.70
Densification Parameter		0.88	0.85	0.94

Cylindrical compacts prepared by mixed powders, sintered at 1460°C, 1h, H_2 atmosphere (Compaction Pressure – 200MPa)

Parameters		Alloys		
		80W-12Ni-8Cu	80W-14Ni-6Cu	80W-16Ni-4Cu
Height (cm)	Green	0.45	0.47	0.37
Diameter (cm)	Green	1.273	1.272	1.271
Weight (g)	Green	5.2314	5.6656	4.4099
	Sintered	5.21	5.66	4.40
Volume (cm^3)	Green	0.57	0.60	0.47
	Sintered	0.36	0.40	0.32
Density (g/cm^3)	Green	9.18	9.41	9.40
	Sintered	14.49	14.30	13.65
% Theo. Density	Green	58.65	60.13	60.06
	Sintered	92.60	91.38	87.23
Densification Parameter		0.8206	0.7835	0.6803

Cylindrical compacts prepared by mixed powders, sintered at 1460°C, 1h, H_2 atmosphere (Compaction Pressure – 200MPa)

Parameters		Alloys		
		85W-9Ni-6Cu	85W-10.5Ni-4.5Cu	85W-12Ni-3Cu
Height (cm)	Green	0.45	0.50	0.43
Diameter (cm)	Green	0.804	0.804	0.804
Weight (g)	Green	2.162	2.446	2.054
	Sintered	2.14	2.42	2.03
Volume (cm^3)	Green	0.23	0.26	0.22
	Sintered	0.15	0.17	0.14
Density (g/cm^3)	Green	9.57	9.58	9.35
	Sintered	14.20	14.19	14.11
% Theo. Density	Green	58.27	58.34	56.91
	Sintered	86.45	86.38	85.91
Densification Parameter		0.6754	0.6730	0.6731

Parameters		Alloys		
		90W-6Ni-4Cu	90W-7Ni-3Cu	90W-8Ni-2Cu
Height (cm)	Green	0.29	0.49	0.43
Diameter (cm)	Green	0.804	0.804	0.804
Weight (g)	Green	1.464	2.471	2.511
	Sintered	1.46	2.46	2.51
Volume (cm^3)	Green	0.15	0.25	0.22
	Sintered	0.09	0.15	0.15
Density (g/cm^3)	Green	10.05	10.00	11.56
	Sintered	16.66	16.40	16.95
% Theo. Density	Green	58.14	57.85	66.88
	Sintered	96.37	94.89	98.08
Densification Parameter		0.9132	0.8787	0.9420

Appendix III

Macro-Hardness of compacts prepared by mixed powders, sintered at 1360°C, 1h, H_2 atmosphere.
(Compaction pressure 200MPa)

Alloys	No. of Observation	D_1	D_2	Hardness $HV_{0.5}$	Average Hardness
80W-12Ni-8Cu	1	59.5	61.8	252	300.2
	2	66.8	66.5	209	
	3	47.8	55.5	384	
	4	49.2	53.6	351	
	5	52.9	56.9	308	
80W-14Ni-6Cu	1	51.2	51.2	354	319.4
	2	58.1	66.3	240	
	3	56.3	51.9	317	
	4	49.6	51.6	362	
	5	54.3	52.7	324	
80W-16Ni-4Cu	1	65.0	79.6	177	299.2
	2	51.5	52.2	345	
	3	52.0	53.3	334	
	4	53.1	53.6	326	
	5	54.4	54.3	314	
85W-9Ni-6Cu	1	48.2	47.1	408	379.2
	2	53.7	50.1	344	
	3	51.0	50.6	359	
	4	52.4	51.2	346	
	5	43.9	48.0	439	
85W-10.5Ni-4.5Cu	1	53.4	54.8	317	287.9
	2	99.7	97.4	95.4	
	3	51.1	54.4	333	
	4	52.3	54.4	328	
	5	49.5	51.1	366	
85W-12Ni-3Cu	1	102.9	110	81.8	79.9
	2	95.6	113.2	85.1	
	3	113.8	99.6	81.4	
	4	108.4	107.7	79.4	
	5	115.3	112.1	71.7	

Macro-Hardness of compacts prepared by mixed powders, sintered at 1360°C, 1h, H_2 atmosphere.
(Compaction pressure 200MPa)

Alloys	No. of Observation	D_1	D_2	Hardness $HV_{0.5}$	Average Hardness
90W-6Ni-4Cu	1	112.8	108.7	75.6	79.4
	2	103.4	111.2	80.5	
	3	98.1	106.6	88.5	
	4	113.5	103.9	78.5	
	5	111.3	113.0	73.7	
90W-7Ni-3Cu	1	95.3	97.7	99.5	99.9
	2	98.8	101.0	92.9	
	3	77.2	92.0	130	
	4	107.6	109.5	78.7	
	5	95.0	98.9	98.6	
90W-8Ni-2Cu	1	93.5	102.4	96.5	99.0
	2	96.8	86.1	111.0	
	3	94.4	99.5	98.6	
	4	98.8	96.4	97.8	
	5	96.5	105.6	90.9	

Appendix IV

Macro-Hardness of compacts prepared by mixed powders, sintered at 1440°C, 1h, H_2 atmosphere.
(Compaction pressure 200MPa)

Alloys	No. of Observation	D_1	D_2	Hardness $HV_{0.5}$	Average Hardness
80W-12Ni-8Cu	1	53.7	55.5	311	294.8
	2	53.6	56.5	306	
	3	56.3	57.7	285	
	4	59.4	55.7	280	
	5	56.6	55.8	292	
80W-14Ni-6Cu	1	46.0	48.3	417	317.4
	2	55.2	56.9	295	
	3	55.0	55.6	303	
	4	60.4	60.1	255	
	5	53.1	55.1	317	
80W-16Ni-4Cu	1	44.7	44.9	462	400.0
	2	46.8	46.5	426	
	3	50.6	52.5	349	
	4	51.3	51.7	350	
	5	47.4	47.3	413	
85W-9Ni-6Cu	1	49.4	52.4	358	347.6
	2	51.1	56.5	320	
	3	54.3	50.3	339	
	4	51.7	49.8	360	
	5	53.6	47.7	361	
85W-10.5Ni-4.5Cu	1	56.9	57.8	282	311.8
	2	52.3	53.3	333	
	3	54.3	54.4	314	
	4	54.3	52.7	324	
	5	53.6	56.5	306	
85W-12Ni-3Cu	1	50.0	51.0	363	383
	2	48.7	48.6	392	
	3	51.2	51.0	355	
	4	48.4	47.5	403	
	5	45.6	50.5	402	

Macro-Hardness of compacts prepared by mixed powders, sintered at 1440°C, 1h, H_2 atmosphere.
(Compaction pressure 200MPa)

Alloys	No. of Observation	D_1	D_2	Hardness $HV_{0.5}$	Average Hardness
90W-6Ni-4Cu	1	46.4	46.9	426	416.4
	2	48.0	45.8	421	
	3	48.5	49.6	385	
	4	46.7	50.7	391	
	5	45.4	44.4	459	
90W-7Ni-3Cu	1	52.3	49.7	356	323
	2	51.4	47.6	378	
	3	57.6	58.0	277	
	4	56.4	56.6	290	
	5	55.8	52.8	314	
90W-8Ni-2Cu	1	45.3	50.2	407	387.8
	2	49.0	49.8	380	
	3	49.7	47.3	394	
	4	48.6	47.4	402	
	5	57.5	50.6	356	

Macro-Hardness of compacts prepared by mixed powders, sintered at 1460°C, 1h, H_2 atmosphere.
(Compaction pressure 200MPa)

Alloys	No. of Observation	D_1	D_2	Hardness $HV_{0.5}$	Average Hardness
80W-12Ni-8Cu	1	71.3	76.0	171	255.8
	2	72.2	71.9	179	
	3	54.4	55.5	307	
	4	50.1	54.1	342	
	5	56.6	58.5	280	
80W-14Ni-6Cu	1	51.6	53.2	338	345.2
	2	57.0	52.8	308	
	3	49.8	49.5	376	
	4	49.5	49.5	378	
	5	52.1	54.5	326	
80W-16Ni-4Cu	1	48.9	52.8	359	347.4
	2	54.8	53.2	318	
	3	52.0	53.1	336	
	4	50.9	48.7	374	
	5	50.8	52.2	350	
85W-9Ni-6Cu	1	56.0	55.5	298	272
	2	56.4	55.2	298	
	3	56.6	55.0	298	
	4	54.6	53.6	317	
	5	79.9	77.7	149	
85W-10.5Ni-4.5Cu	1	46.1	48.3	416	363.2
	2	61.4	61.6	249	
	3	50.9	50.2	363	
	4	48.0	49.4	391	
	5	48.8	47.9	397	
85W-12Ni-3Cu	1	51.4	53.7	336	321.4
	2	53.4	54.3	320	
	3	52.9	54.6	321	
	4	55.2	55.3	304	
	5	52.1	54.5	326	

Alloys	No. of Observation	D_1	D_2	Hardness $HV_{0.5}$	Average Hardness
90W-6Ni-4Cu	1	60.5	60.3	254	288.8
	2	47.5	49.2	397	
	3	53.9	52.6	327	
	4	64.6	64.8	221	
	5	61.4	61.5	245	
90W-7Ni-3Cu	1	56.0	57.4	288	292.2
	2	52.8	55.0	319	
	3	57.2	58.3	278	
	4	52.9	55.1	318	
	5	59.8	60.1	258	
90W-8Ni-2Cu	1	60.4	63.9	240	328.8
	2	53.1	51.6	338	
	3	55.2	50.3	333	
	4	48.3	50.4	381	
	5	49.3	53.3	352	

Appendix V

Micro-Hardness of compacts prepared by mixed powder, sintered at 1440°C, 1h, H_2 atmosphere (Compaction Pressure 200MPa)

Alloy	NO. of Obs.	Tungsten				Matrix			
		D_1	D_2	$HV_{0.05}$	Ave. $HV_{0.05}$	D_1	D_2	$HV_{0.005}$	Ave $HV_{0.005}$
80W-12Ni-8Cu	1	18.0	18.2	283	373.4	9.0	9.2	112.0	101.56
	2	15.5	15.3	391		10.4	10.2	89.1	
	3	15.4	15.4	391		8.8	8.8	120	
	4	15.2	15.2	401		10.0	9.8	94	
	5	15.1	15.3	401		10.0	10.0	92.7	
80W-14Ni-6Cu	1	15.2	15.0	407	401.2	9.5	9.4	105	113.1
	2	14.7	15.0	423		9.8	9.7	98.5	
	3	14.8	14.8	423		8.5	8.7	125	
	4	15.7	15.4	386		9.0	9.2	112.0	
	5	16.0	15.8	367		8.6	8.6	125	
80W-16Ni-4Cu	1	15.2	15.3	401	446.6	8.4	8.4	131.0	134.6
	2	13.8	14.2	473		8.0	8.1	145.0	
	3	15.0	15.0	412		8.6	8.5	128.0	
	4	13.8	13.8	487		8.1	8.1	141.0	
	5	14.2	14.2	460		8.4	8.6	128.0	

Micro-Hardness of compacts prepared by mixed powder, sintered at 1440°C, 1h, H_2 atmosphere (Compaction Pressure 200MPa)

Alloy	NO. of Obs.	Tungsten				Matrix			
		D_1	D_2	$HV_{0.05}$	Ave. $HV_{0.05}$	D_1	D_2	$HV_{0.005}$	Ave. $HV_{0.005}$
85W-9Ni-6Cu	1	14.4	14.4	447	448.4	11.4	11.5	71.3	85.28
	2	14.5	14.6	441		10.2	10.0	90.9	
	3	14.4	14.3	453		10.5	10.5	84.1	
	4	14.6	14.6	435		10.0	10.0	92.7	
	5	14.2	14.0	466		10.4	10.3	87.4	
85W-10.5Ni-4.5Cu	1	15.0	14.1	441	359.2	10.8	10.4	82.5	88.56
	2	14.1	13.7	480		10.5	10.6	84.1	
	3	14.8	14.7	429		10.5	10.7	82.5	
	4	14.4	14.1	460		9.5	9.7	101	
	5	15.9	15.1	386		9.9	10.1	92.7	
85W-12Ni-3Cu	1	16.0	16.0	362	424	10.5	10.7	82.5	96.38
	2	14.4	14.6	441		10.0	10.2	90.9	
	3	14.6	14.6	435		9.6	9.8	98.5	
	4	14.4	14.7	441		9.2	9.6	105	
	5	14.5	14.5	441		9.4	9.4	105	

Micro-Hardness of compacts prepared by mixed powder, sintered at 1440°C, 1h, H_2 atmosphere (Compaction Pressure 200MPa)

Alloy	NO. of Obs.	Tungsten				Matrix			
		D_1	D_2	$HV_{0.05}$	Ave. $HV_{0.05}$	D_1	D_2	$HV_{0.005}$	Ave. $HV_{0.005}$
90W-6Ni-4Cu	1	14.2	14.0	466	459.4	9.8	9.8	96	96
	2	15.0	15.2	407		9.5	9.6	103	
	3	14.0	14.1	473		10.2	10.0	90.9	
	4	13.5	13.3	516		9.5	9.7	101	
	5	14.6	14.6	435		10.4	10.0	89.1	
90W-7Ni-3Cu	1	16.0	15.8	367	356.2	10.2	10.4	87.4	90.16
	2	16.2	16.3	353		9.7	9.6	101.0	
	3	16.4	16.4	345		10.4	10.3	87.4	
	4	16.0	16.2	358		10.0	10.2	90.9	
	5	16.1	16.1	358		10.5	10.5	84.1	
90W-8Ni-2Cu	1	15.5	15.7	381	360.4	10.0	9.9	94	86.78
	2	16.6	15.8	353		9.0	9.2	112	
	3	17.5	15.5	340		9.5	9.0	110	
	4	14.6	14.8	429		8.9	9.3	112	
	5	17.5	17.7	299		10.2	10.1	90.9	

Micro-Hardness of compacts prepared by mixed powder, sintered at 1460°C, 1h, H_2 atmosphere (Compaction Pressure 200MPa)

Alloy	NO. of Obs.	Tungsten				Matrix			
		D_1	D_2	$HV_{0.05}$	Ave. $HV_{0.05}$	D_1	D_2	$HV_{0.005}$	Ave $HV_{0.005}$
80W-12Ni-8Cu	1	15.5	15.6	386	415.2	11.0	11.2	75.2	100.34
	2	14.5	14.6	441		8.8	9.0	120.0	
	3	15.2	15.2	401		9.5	9.5	103	
	4	15.0	15.2	407		9.4	9.4	105	
	5	14.5	14.5	441		9.8	9.6	98.5	
80W-14Ni-6Cu	1	14.7	14.7	429	401.2	9.5	9.5	103	107.3
	2	17.5	17.0	313		9.8	9.6	98.5	
	3	14.8	14.7	429		9.2	9.0	112	
	4	15.0	15.1	412		9.0	8.8	118	
	5.	14.9	14.7	423		9.4	9.4	105	
80W-16Ni-4Cu	1	15.2	15.2	401	402.4	10.2	10.0	90.9	102.38
	2	15.2	15.3	401		9.2	9.2	110.0	
	3	15.4	15.3	396		9.5	9.7	101.0	
	4	15.1	15.1	407		9.5	9.6	103.0	
	5	15.2	15.0	407		9.2	9.4	107.0	

Micro-Hardness of compacts prepared by mixed powder, sintered at 1460°C, 1h, H_2 atmosphere (Compaction Pressure 200MPa)

Alloy	NO. of Obs.	Tungsten				Matrix			
		D_1	D_2	$HV_{0.05}$	Ave. $HV_{0.05}$	D_1	D_2	$HV_{0.005}$	Ave. $HV_{0.005}$
85W-9Ni-6Cu	1	16.2	16.0	358	383.6	8.5	8.8	125	102.18
	2	16.0	15.8	367		9.5	9.3	105	
	3	15.2	15.3	401		9.8	9.9	96	
	4	15.0	15.0	401		10.2	10.0	90.9	
	5	15.4	15.4	391		10.0	9.8	94	
85W-10.5Ni-4.5Cu	1	16.0	16.2	358	372.2	10.4	10.5	85.7	88.06
	2	16.0	16.0	362		10.2	10.2	89.1	
	3	15.2	15.4	401		10.0	9.8	94.0	
	4	16.4	16.3	349		10.6	10.5	84.1	
	5	15.4	15.4	391		10.3	10.4	87.4	
85W-12Ni-3Cu	1	14.0	14.1	473	430.0	10.0	10.4	89.1	88.92
	2	14.0	14.0	473		9.8	10.0	94	
	3	14.0	14.4	460		10.8	11.6	73.9	
	4	14.5	14.5	441		9.6	9.8	98.5	
	5	17.6	17.4	303		10.0	10.4	89.1	

Micro-Hardness of compacts prepared by mixed powder, sintered at 1460°C, 1h, H_2 atmosphere (Compaction Pressure 200MPa)

Alloy	NO. of Obs.	Tungsten				Matrix			
		D_1	D_2	$HV_{0.05}$	Ave. $HV_{0.05}$	D_1	D_2	$HV_{0.005}$	Ave. $HV_{0.005}$
90W-6Ni-4Cu	1	15.0	15.1	412	424.4	11.5	11.2	72.6	84.12
	2	14.2	14.2	460		10.0	10.2	90.9	
	3	15.6	15.4	386		10.8	10.8	79	
	4	14.8	14.8	423		10.0	9.8	94	
	5	14.5	14.5	441		10.4	10.6	84.1	
90W-7Ni-3Cu	1	15.5	16.0	376	358.8	9.0	9.0	115	115.6
	2	16.0	16.5	353		9.5	9.5	103	
	3	15.5	15.5	386		8.5	9.0	122	
	4	17.5	17.5	303		8.5	8.5	128	
	5	16.0	15.5	376		9.5	9.0	110	
90W-8Ni-2Cu	1	14.9	16.2	386	381	8.5	8.1	135	104.2
	2	14.9	15.3	407		8.9	8.6	122	
	3	15.8	15.9	371		9.6	9.7	101	
	4	15.0	15.4	401		10.0	11.4	81	
	5	15.9	16.2	340		10.5	10.8	82